# Interactive comment on "Vertical Wind Velocity Measurements using a 5-hole Probe with Remotely Piloted Aircraft to Study Aerosol-Cloud Interactions"

Response to anonymous referee #1

## General comments

Both reviewers' responses focus primarily on the method in which the calibration procedure and simplified equations of motion have been presented in this manuscript. One of the main concerns is that we have applied a simplified calibration and calculations of atmospheric winds when full equations have long been published (Lenschow et al., 1989). We are well aware of the Lenschow equations. We are also aware (but did not clearly state in the manuscript) that we are presenting results from a quasi-linear response region of the 5-hole probe, and we had made a conscience choice to structure the manuscript this way. As both reviewers asked for clarification regarding the calibrations and equations of motion, we have modified the manuscript with citations for the full set of equations (Lenschow et al. (1989); Boiffier (1998); Kroonenberg et al. (2008)) and simply mention in the manuscript that when operating within a linear regime (ca. $\pm$ 10 degrees), and that simplified equations may be used for evaluating results and assessing uncertainties of atmospheric wind measurements. We also show in the responses here and in the manuscript, that the main results related to the power spectra, calculation of turbulent kinetic energy and the atmospheric winds do not change for our flight conditions, even after accounting for nonlinearity in the calibration coefficients and the full set of Lenschow equations.

We also highlight that this manuscript presents results using a commercially-available probe with custom electronics, and an INS and RPA that have not been previously reported in the literature. Consequently, we dedicate a section of the manuscript to the calibration/validation of the 5-hole probe in order to compare with other multi-hole probes in the literature. As the 5-hole probe and associated sensors, the INS, and the RPA comprise the measurement system, all components should be validated together as a system. We present the results of turbulent kinetic energy (TKE) in order to compare our results to other such RPA measurements (i.e., Båserud et al. (2016); Lampert et al. (2016); Canut et al. (2016)). We are not aware of any direct comparisons of vertical wind velocity between ground-based remote-sensing instruments (e.g., lidar, cloud radar) and a multi-hole probe mounted on a RPA. The vertical winds derived from the 5-hole probe have been implemented in aerosol-cloud parcel models (e.g., Sanchez et al. (2017)), and measurements of updraft velocity to within 0.1 m $s^{-1}$ are largely sufficient for conducting aerosol-cloud closure studies. As the focus of this work is obtaining updraft measurements, we have updated the title of

the manuscript to reflect this. Finally, we included a new section that describes the sensitivity of vertical velocity distributions on resulting cloud droplet number concentrations.

## Specific comments

The same method is used to name page and line number : page/line. Comments from the reviewer appear in italic, response from the authors follows as well as the updated section of the manuscript. However, as the manuscript has undergone significant changes, we invite the reviewers to directly refer to the updated version of the manuscript for specified sections.

RPAS (Remotely Piloted Aircraft System) is used to name the global system, including aircraft + ground control station, and RPA (Remotely Piloted Aircraft) only refers to the aircraft.

**2/6: 'INS measures six axes': No! It measures 3 linear and 3 circular accelerations or motions.*

Response: We are clearly referring to the six degrees of freedom of the INS (as noted by the reviewer; three linear and three rotational). These six degrees of freedom are often denoted as six-axis sensors by the manufacturers (i.e., TDK, Bosch) and peer-reviewed literature in robotics. Nonetheless, we will remove the sentence in the manuscript to avoid any confusion.

In the manuscript at 2/6 : "INS measure linear and rotational motion of the aircraft (or unmanned aerial system) and are used to back out wind vectors in the Earth's coordinate system."

**2/14: Having a look in Reuder 2008 shows: SUMO was not able to measure the wind vector. Actually it had no flow sensors aboard at that time. Wind speed and direction were estimated by the drift of the aircraft, instead. An early example of a small and light RPA that actually measured the wind vector was published by Spiess et al in 2007 (already in the list of references).*

Response : We thank the reviewer for pointing this out and we have updated the manuscript to cite Spiess et al. (2007). We also clarify that Reuder et al. (2008) do not calculate wind speed and direction by the drift of the RPA, rather a vector calculation using minimum and maximum ground speeds and respective orientations along a circular path around a fixed GPS coordinate.

In the manuscript at 2/5 sentence now reads : "to ultra-light unmanned aerial systems (i.e., $M^2AV$; Spiess et al (2007))." and at 2/14 : "to a 600 g SUMO (Reuder et al., 2012)"

**2/19: very unusual and confusing way to cite articles: M2AV-Spiess and MASCWildmann! So, the authors names were Spiess (2007) and Wildmann (2014). Aircraft described in these articles were named M2AV and MASC. Please correct!*

Response : Description of RPAS has been re-formulated as the reviewer suggested.

** 2/22: Having a look at the sophisticated error analysis of van den Kroonenberg et al (2008), I doubt that Thomas et al (2012) and Baserud (2014) measured the vertical wind 5 times more accurately, the latter with a*

*much simplier measurement system. Please explain how this was possible!*

Response : The uncertainty associated with the wind measurement is a combination of the errors from the probe and the INS. Thomas et al. (2012) and Reineman et al. (2013) use much more precise INS which allow them to report smaller uncertainties. Even if Båserud et al. (2016) and Thomas et al. (2012) both implemented an Aeroprobe instrument (membrane-based sensors), the uncertainties reported in their respective papers are not comparable. Båserud et al. (2016) did not include the INS error in the estimation of the wind uncertainty. We have clarified this in the manuscript. Updates on the wind uncertainty from RPAs and the method to obtain it are provided in the manuscript (see next two comments for updated text).

** 2/26 Now measurement of the vertical wind seems to become 20 times more accurate. Explain how this was possible!*

Response: The increase in accuracy is largely due to the INS model selected for wind measurements. The following uncertainties are provided by Reineman et al. (2013) for the dGPS/IMU on board of the Manta RPA, 0.007/0.007/0.011 degrees for roll/pitch/heading, respectively, and 0.01 m/s for the INS vertical velocity. The uncertainties for the INS on the $M^2AV$ (Kroonenberg et al., 2008), are higher, 0.54/0.71/1.22 degrees for roll/pitch/heading, respectively, and 0.58 m/s for the INS vertical velocity. All these parameters present in Reineman et al. (2013) composed a system similar to the BAT probe mounted on a small manned aircraft (Garman et al. (2006), Crawford et al. (1992)).

**Are these accuracies (from 2/16 to 2/26) all the same by mathematical definition? Do you mean absolute accuracies of the mean vertical wind or resolving turbulent fluctuations? How are the various precisions for the wind velocities in the referenced literature calculated? Are they comparable with each other?*

Response : As the reviewer suggests, the reported uncertainties are not necessarily consistent by the same mathematical definition and a complete analysis is beyond the scope of this paper. Indeed, this is an important point, which we have attempted to clarify this in the manuscript.

In the manuscript 2/14 :"A wide range of remotely piloted aircraft (RPA)[1] has been used to measure atmospheric winds, from a 600 g SUMO (Reuder et al., 2012) to a 30 kg Manta (Thomas et al., 2012). In particular, a multi-hole probe paired with an INS has been the main mechanism for obtaining vertical winds in fixed-wing RPA. Ultimately, the combination of the multi-hole probe, pressure sensors, and the INS dictate the precision of atmospheric wind measurements. The following accuracies for vertical wind measurements $w$ were reported in the literature for different RPA platforms; they were obtained by different methods, which provided either 1-sigma uncertainty or systematic error analysis associated with a specific pair of probe/INS. In Kroonenberg et al. (2008), a custom 5-hole probe on the $M^2AV$, implemented with a GPS-MEMS-IMU was reported with an accuracy for $w$ within $\pm$ 0.5 m $s^{-1}$. The accuracy was based on a systematic error estimation using characteristic flight parameters with a reference state of $w$ = 1 m $s^{-1}$. The uncertainty in $w$ reported for the SUMO (Reuder et al., 2016) is $\pm$ 0.1 m $s^{-1}$ as given by the manufacturer (Aeroprobe Corporation); however, the impact of the INS was not included in their analysis. In Thomas et al. (2012), the Manta RPA was also equipped with a commercial Aeroprobe and a C-Migits-III INS to obtain a minimum resolvable $w$ of 0.17 m $s^{-1}$ (1-sigma). The

[1]RPA refers to the aircraft, as RPAS represents the airframe and the ground control station

uncertainty analysis was based on a Gaussian error propagation described in Garman et al. (2006). The Manta and ScanEagle RPAs described in Reineman et al. (2013) achieved precise wind measurements with a custom 9-hole probe and NovAtel INS with reported uncertainties for $w$ within $\pm$ 0.021 m $s^{-1}$. Their uncertainty was obtained from a Monte-Carlo simulation, and was also consistent with reverse-heading maneuvers. The higher precision reported in the latter study (Reineman et al., 2013) is related to probe design and the high precision of the INS. The vertical wind measurements in Reineman et al. (2013) have a similar performance as reported with the BAT probe ("Best Air Turbulence Probe") on a small piloted aircraft (Garman et al., 2006)."

** 2/30 What do you mean with '(4) improved algorithms for wind field estimation from dynamic soaring'?*

Response : Elston et al. (2015) reviewed RPAS in atmospheric science and included methods for wind field estimation based on dynamic soaring. We have removed this point as it does not relate directly to our manuscript.

** 4/19 Indeed, it is possible to use a 5-hole probe with only three differential pressure sensors. But considering publications e.g. by the American Institute of Aeronautics and Astronautics (look for Weiss et al. 1999 to 2002), using 5 differential pressure sensors increases accuracy (measuring the pressure difference of the 5 holes relative to a combined reference), significantly. Since a pressure sensor is light and cheap, can you explain why you decided to use only three?*

Response : There exist multiple methods for configuring the pressure sensors as described in peer-review literature. Wildmann et al. (2014) present two possibilities implemented on the $M^2AV$ (fig.4) and on the MASC (fig.5). Reineman et al. (2013) use a similar differential pressure configuration as the present study. The five pressure sensor system used by Reineman et al. (2013) measured two additional axes (9 holes with a 45 degree component between vertical and horizontal axes) to improve performance of their probe. Three differential pressure measurements method is also proposed by the Aeroprobe Corporation (calibration files provided by the manufacturer) as well as the 5 hole-probe implemented by Thomas et al. (2012) on the Manta and Reuder et al. (2016) on the SUMO. Adding five differential pressure sensors is only a valid argument if the sum of the measurement errors of the individual sensors is less than a single sensor (which would not be the case for the sensors that we are using). In addition, using five differential pressure sensors requires additional resources on the data acquisition system (which we did not have), and more volume in the payload bay (an extra printed circuit board).

** 4/10ff (section 2.2) Using a 5-hole probe also requires a proper tubing strategy, see Wildmann et al (2014), in order to avoid signal damping and acoustic tube resonance. Can you please explain how did you take care of tubing issues?*

Response : Indeed, we are aware of the tubing issues extensively studied in Wildmann et al. (2014). In the present study, the tubing length is less than 15 cm, and the inner diameter is 0.1 mm, which are dimensions similar to Wildmann et al. (2014); and the frequency of our measurements is less than that verified by Wildmann et al. (2014). We have specified this in the manuscript.

**Summing up section 2.2: Why don't you apply well known, state-of-the-art and published (e.g. articles that are already in your list, by van den Kroonenberg and Wildmann et al.) methods for tubing your 5-hole probe? Or in other words: What are the advantages of your unusual method? And can you show that the results are still good enough?*

Response : As noted in the opening statements of our response, we were operating in the nearly linear response regime of the probe. In addition, we used a configuration proposed by the manufacturer of the probe and methods that are also described in a thesis by Truong (2011). None of the results in this manuscript (PSD, TKE, updraft) significantly change when using the full expressions reported in Kroonenberg et al. (2008) and Wildmann et al. (2014) because we operated the probe within a quasi-linear regime (at small pitch and roll angles). Nonetheless, we recognize that a thesis and manufacturer's procedures are not as easily accessible as peer-reviewed literature. Consequently, we have updated Section 2.2 with citations to Wildmann et al. (2014), whose procedures are similar to those used in our manuscript. The calibration of the probe in the wind tunnel (Section 3), as well as the Cal/Val with the sonic anemometer (Section 4) and cloud radar (Section 5) confirm the probe's performance.

*4/20 'hole 1 measures the total pressure' - No! And this is a substantial mistake. Since the stagnation point (angle of attack and side slip, nalpha and nbeta being not zero) is *somewhere* on the spherical surface of the 5-hole probe, hole 1 does not represent the total pressure! Doing this mistake, the following discussion of wind measurements and accuracies is pointless!*

Response : P1 is referred as the total pressure (Truong, 2011) or as the pressure at the stagnation point (Reineman et al., 2013). To be consistent with the reviewer's comments, P1 is denoted as the pressure at the stagnation point in the manuscript, and Fig.1.a is updated. An update of the calibration method has been provided in responses of comments about Section 3.1.

** 4/24f No. An IMU measures accelerations (3 linear and 3 circular). An INS combines an IMU with GPS, usually using a Kalman filter.*

Response : In the literature INS or IMU are sometimes used incorrectly for the same meaning. The manuscript has been updated to use INS to refer to the system that combines an IMU with GPS.

** 4/29 'plane'. You mean aircraft or aeroplane*

Response : To be consistent with the text, the terms "RPA" or "RPAS" are used.

In the manuscript 5/5, "the measured motion of the RPA (given by the INS)".

**5/1: No! The Eulerian angles are NOT given in the aircraft coordinate system, but in the Earth's coordinate system. This is why people invented INS. And this is important, if you want to measure the atmospheric wind using an aircraft!*

Response : Indeed, the Eulerian angles are neither given in the aircraft coordinate system nor in the Earth's coordinate system. They represent the orientation of the aircraft with respect to the Earth's coordinate system and build the transformation matrix to convert angles and velocity from one coordinate system to another. We have clarified this point in the manuscript.

In the manuscript 5/6: "The angle of attack, the angle of sideslip, and the airspeed $V_a$ are measured by the 5-hole probe in the probe coordinate system and then transform to the RPA coordinate system; while the attitude angles from the INS provide the transformation of $\alpha$, $\beta$ and $V_a$ from the RPA coordinate system to the Earth's coordinate system. Lenschow equations (Lenschow and Spyers-Duran, 1989) are therefore followed to calculate the wind vector in the Earth's coordinate system. "

** Entire section 2.3 (page 5): So, you have an INS that delivers the Eulerian angles (roll, pitch, heading). And you have a 5-hole probe that (when properly tubed and calibrated) delivers angle of attack and side slip (nalpha and nbeta) as well as the total pressure (although you will not have them with the methods described in the manuscript ...). Now you can apply the exact equations, published since the 1970ies, also by Don Lenschow and others, without having to apply any simplification or estimation that only causes worse data. To have a nice and short overview on how to do this, please read (and apply) van den Kroonenberg et al (2008).*

Response : As stated previously, we are well aware of the exact equations, as well as the limits of the simplified equations. Consequently, we specifically designed the experiment to follow straight-and-level flight legs. Pitch and roll were almost always less than $\pm$ 10 degrees, which is in a quasi-linear response regime of the multi-hole probe. A comparison of the three wind components, $u, v, w$, calculated with the complete Lenschow equations and with the simplified equations has been conducted on straight-and-level legs for the five flights at CRA, Lannemezan. The mean value of the difference in the calculated winds between complete and full equations is less than 0.03 $\pm$ 0.05 m/s. The difference is less than the uncertainty based on the wind tunnel calibration.

** 5/4 Even straight and level flights have varying Eulerian angles. Roll and especially pitch are not zero! The simplified equation (1) for the wind vector possibly holds 1) for heavy and large manned aircraft (talking about airliners) that are less dynamic during flight, and 2) probably only for the estimation of the mean wind vector. But a tiny RPA as used in the presented study is heavily agile. Reading the manuscript I do not see any reason not to use the precise equations (again, see e.g. van den Kroonenberg et al.), or is there any?*

Response : The reviewer is rightfully concerned about the stability of the RPA, and maximum pitch and roll for the five flights in Lannemezan have been investigated. The roll angle exceeds 10 degrees less than 1% of the time, except for Flight 4 (unstable flight close to stall speed) where roll exceed 10 degrees up to 2 % of the time. The pitch angle never exceeded 10 degrees except when it approached stall speed (Flight 4) – even then, pitch angles did not exceed 10 degrees during the straight-and-level legs more than 0.1 % of the time.

** 5/11 $V_e$ etc is confusing. Why don't you use $(V_x, V_y, V_z)$ or $(U, V, W)$ for the groundspeed vector, since you defined your Earth coordinate system in the same paragraph using (x,y,z)?*

Response : We agree. In the manuscript $V_p$ for the RPA vertical speed has been replaced by $V_z$.

** 6/1 Eq. (2) is not correct. The pressure differences in the denominators have to be divided by the dynamic pressure enhancement, which is the difference between the total and the static pressure. Hole 1 does not deliver the total pressure! See above.*

Response : As stated previously, the method described in the manuscript follows the Aeroprobe corporation calibration file. However, to be consistent with the peer-reviewed literature, the calibration in the manuscript has been updated from the Aeroprobe corporation method to the Treaster et al. (1978) method, also used in Wildmann et al. (2014). A polynomial fit has been obtained from $C_\alpha$ and $C_\beta$ to calculate $\alpha$ and $\beta$. The difference between the previous calibration method and the updated results of the angles is small for angles within ca. $\pm$ 10 degrees.

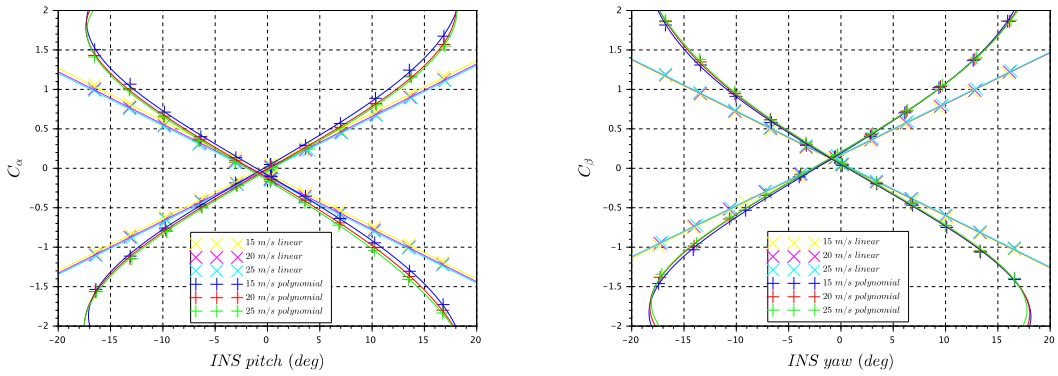


(a) (b)

Figure 1: Comparison of the previous calibration with the Aeroprobe calibration method and the updated calibration with method from Treaster et al. (1978) for (a) $C_\alpha$ and (b) $C_\beta$.

** 6/6 Where does Eq. (3) come from? Please cite literature!*

Response : Equation (3) comes from the Aeroprobe calibration file, and can also be found in the literature (Truong, 2011). As noted earlier, we have updated the equations and cited Wildmann et al. (2014).

** 6/21: Why do you need a linear relation between $C_\alpha$/ $C_\beta$ and alpha/beta? This is leading to the question how alpha and beta are calculated from the calibration to obtain the wind vector components. Using the system e.g. described in Wildmann (2014), alpha/beta of up to +-20 degree can be used and a polynomial fit accounts for potential asymmetry of the probe's tip structure.*

Response : Figure 4 in the manuscript has been updated with the new $C_\alpha$ and $C_\beta$.

** Entire section 3.1: There is no need to invent the wheel once more. How to calculate the wind vector and how to calibrate a 5-hole probe is well published and explained. For example in articles in your list of references, see again van den Kroonenberg (2008), there: page 1972f, Eq. (1) to (13).*

Response: As mentioned, we are using a commercially available 5-hole probe (Aeroprobe) with custom electronics. We are well aware of assumptions that have been made; however, due to our configuration of pressure sensors and tubing, we have revised our calibration using the Treaster et al. (1978) method (used in Wildmann et al. (2014)), rather than the method based on Bohn et al. (1975) (used in Kroonenberg et al. (2008)).

**7/7ff: Again, the pressures measured on the dynamic and static pressure holes of the 5-hole probe (in your manuscript delta(P1-P6) and Ps=P6) change with alpha and beta. Moreover other work shows, that the static port of five hole probes fluctuate for inclined inflow.*

Response : The coefficients $C_q$ and $C_s$ from the Treaster et al. (1978), and Wildmann et al. (2014), are calculated to obtain the airspeed as a function of $\alpha$ and $\beta$ for our probe (Fig.2). The airspeed is then calculated with $P_s$ and $P_q$ (Table A1 in Wildmann et al. (2014)) from (Anderson, 2001) with speed of sound and Mach number, or from (Wildmann et al., 2014) with the Poisson number.

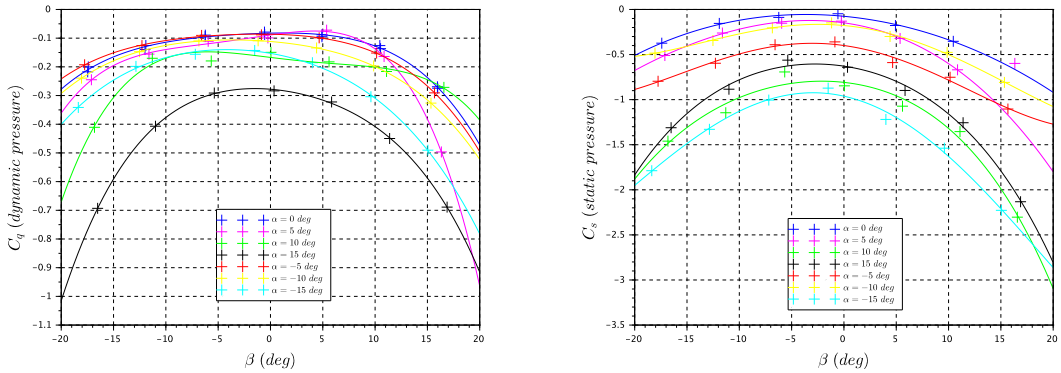


(a) (b)

Figure 2: Dynamic and static pressure coefficients function of angle of sideslip. Crosses correspond to measurement points, and curve to polynomial best fit. The wind tunnel velocity is set up to 15 m $s^{-1}$.

** 7/9 Why did you calibrate with wind speeds between 12 and 34 m/s? Of course, a single calibration of the 5-hole probe (the entire grid, see Fig. 3 and 4) holds only for one airspeed, i.e. the entire procedure has to be repeated in e.g. 1 m/s steps. This leads to the question, how your autopilot system is controlling the air speed of the RPA?*

Response : Variation of the wind tunnel airspeed from 12 to 34 m $s^{-1}$ simply verifies the calibration of the probe in the range of RPA operating airspeed and the instrument uncertainties. The difference between the polynomial fits at distinct airspeeds is relatively small and leads to less than a 0.6 degree difference between $\alpha$ or $\beta$ (Fig.1). The RPAS controls airspeed by pitch adjustment.

** 7/13f: What is "triangular motion applied to the pitch axis of the platform"? Why is that performed?*

Response : Triangular motion is applied to validate the calibration in a controlled environment and verify the response of the INS. The figure (Fig.5 in the manuscript) shows a larger uncertainty related to faster motions induced on the probe and INS. We suspect the increased uncertainty is related to an induced lag in the filtering process within the INS.

** 7/15: Actually Fig. 5 shows plenty of noise, causing a systematic uncertainty of the vertical-wind measurement of about 0.1 m/s. This means turbulent fluctuations in this order of magnitude cannot be resolved by the presented system. Please make this clear!*

Response : We clarify in the text that turbulent fluctuations on the scale of 0.1 m $s^{-1}$ cannot be resolved as shown in Figure 5 in the manuscript.

** Entire section 3.2: Eventually averaging leads to a mean vertical wind about zero. Having in mind the mean vertical wind should be about zero in the ABL if you average long enough, this is ok if you are only interested in the mean wind. But why is there so much noise? Possibly caused by the electronic pressure transducers?*

Response : The averaging is conducting over time scales of the flight, which are sufficiently large. As stated in the response 7/13, the high frequency motions of the two-axis platform increase the noise in $w$ calculation. The uncertainty remains acceptable as the standard deviation of $w$ is less than 0.1 m/s (Fig.5 in the manuscript).

** 7/28 It is the Gaussian propagation of errors, not the maximum error propagation - this should be mentioned!*

Response : The manuscript has been updated and the section 3.2 is named Gaussian error propagation on vertical wind velocity.

** 8/4, Eq. (6a): please define $a_{alpha}$ !*

Response : We thank the reviewer for catching this oversight and have defined $a_{\alpha}$. (see next comment for the updated text)

** 8/5, Eq. (6b): please explain the entire equation!*

Response : The section 3.2 has been rewritten to provide more details and clearer explanation about the conducted uncertainty analysis. Please, refer to 6/29 in the manuscript.

** What is missing in section 3 or 4 is the most simple test to see if the calibration of the system works at least for the mean wind vector: Flying identical legs in opposite direction in a calm atmosphere (e.g. the residual layer, or in an almost neutral stratification under a overcast sky). See also Fig. 6 and Eq. (17) in van den Kroonenberg et al. (2008). Can you show that the heading does not influence the wind measurements?*

Response : Actually, a drift in the heading does influence the horizontal wind calculation. We have flown identical legs in the opposite direction to specifically show that the wind vectors are similar (within the instrument uncertainty). We show a time series of such results here, and state that such verifications have been done in the manuscript. The influence of the drift in the heading is clearly visible in the calculation of the $u$-component of wind, as $u$ increases along each leg (in blue in Fig.3). The uncertainty in horizontal winds is 1.1 m/s.

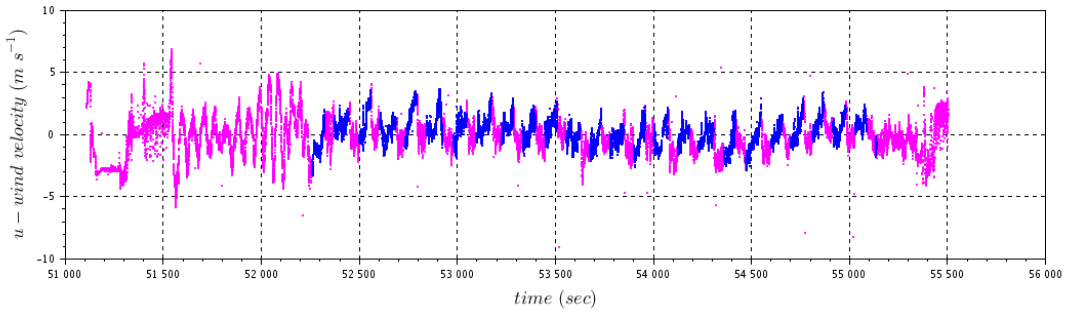


Figure 3: Flight 5 at CRA, Lannemezan, time series of the East-West wind ($u$-component) measured from the wind-RPA. Straight-and-level legs are represented in blue.

** Section 4.1: It is very important to check the power spectra of the resulting wind (of course only if the mean-wind check was ok, i.e. identical legs in opposite direction in a calm atmosphere). Spectra show systematic errors as visible in Fig. 7, above 1 Hz (can be the noise level). These are not mentioned in the manuscript - please do so!*

Response : We are aware of the error visible on the $v$-component above 1 for Flight 1, 2 and 3 (green in Fig.6b in the revised manuscript). However, the error has been removed by reconfigurating the INS as shown in the PSD of Flight 5 (blue in Fig.6b in the revised manuscript) .

*However, the mean spectra in Fig. 7 show two critical issues: 1) the Kolmogorov slope is NOT achieved neither with the sonic nor with the RPA data. I do not agree with your text in 9/7. Your spectra have significant different slope. But this can be caused by not having ideal conditions for a locally isotropic turbulent sub-range.*

Response : The Welch method has been used to plot the PSDs. The slope of the wind PSDs from the RPA data follows the -5/3 line.

*More critical (not acceptable) is the following: 2) the spectral power of the RPA data is by a factor of about*

*5 larger than the spectral power of the sonic. As you mention in 9/8, this was caused by 'the motion of the RPAS'. But if the measured data is governed by the aircraft motion and not by the atmospheric turbulence, any further analysis of turbulence is useless and futile!*

Response : This is a known issue, Reuder et al. (2016) report a SUMO overall energy level that is also higher than that of the sonic anemometer. The reason for the systematic difference has been investigated for the present work, using the decomposition of the wind equations to better understand the influence of each terms : airspeed, ground speeds, heading. Sampling frequencies and new/old calibrations have also been compared without showing any differences in the PSDs. The ground speeds obtained from the INS ($V_x$, $V_y$, $V_z$) present systematic higher energy level for frequencies less than 0.3 Hz. More efforts are going to be invested in selecting the parameters for the extended Kalman filter of the INS, and a comparison with another INS model is going to be conducted to select the best instrument. We recognize that our current measurements are not be suitable for convergence/divergence calculations, however, we demonstrate that for aerosol-cloud interactions, the accuracy achieved with our updraft measurements is valid for estimation of cloud droplet number (Section 6).

** Fig. 8: There is a huge difference between sonic and RPA data around zero vertical wind, please explain!*

Response : The difference around zero vertical wind is simply due to instrument uncertainty reported in Figure 5 in the manuscript. The lower limit in vertical wind measurements is ca. 0.1 m/s.

** Fig. 9: There is a huge difference between mast and RPA data around zero vertical wind. Is there any easy explanation? Section 4.2 is not helpful but confusing.*

Response : We have restructured Section 4 to clarify.

** 9/13 'This step is needed ...' I do not understand this - the attitude of the aircraft and the 5-hole probe (assuming there is no mounting error) is known from the Eulerian angle delivered by the INS. And the mounting error of the probe to the aircraft is constant.*

Response : Throughout the course of a field campaign, we detected relatively small differences in the performance of the probe related to its alignment. Exposure to the sun altered the wing profile and control surfaces, coupled with repeated net landings, the alignment of the probe relative to the airstream did change – consequently we verify/correct for these changes for each flight.

** Section 4.2: What is the intention of this analysis of the TKE? What shall be learned? Why is it filled with corrections? I am quite sure that these considerations become unnecessary after doing a correct wind-vector calculation (see above).*

Response : The analysis of TKE was selected simply to compare the measurements from our RPA to those published from other platforms. Having observed non-isotropy in the RPA's

transversal wind component, we then seek to improve TKE calculations. Such corrections are similar to the method proposed in Lampert et al. (2016) to obtain TKE from the $M^2AV$ platform during the BLLAST campaign.

** 9/30 TKE: From the section 3.3 we know that the uncertainty for the vertical wind is 0.1 m/s. Thus the measurement system causes (possibly by electrical noise) already a standard deviation in this order of magnitude in the data. How large is the uncertainty for the horizontal wind? This is important to know in order to estimate the significance of the presented TKE data.*

Response : The uncertainty in horizontal wind results primarily from drift in the INS heading and is 1.1 m/s (based on out-and-back flights along straight-and-level legs). Note this uncertainty is largely driven by the uncertainty related to the transversal wind component.

** 10/2 I doubt that reported TKE deviations between sonic data and other small RPA is increasing faith into the presented method or is explaining any physics. What is your message here?*

Response : To our knowledge, there is no direct comparison of updraft measurements between a RPA platform and ground-based remote-sensing instruments; consequently, we calculate TKE to compare/validate our wind measurements with previous peer-reviewed results.

** Section 5: The differences and shifts in the distributions shown in Fig. 12 to 15 are mainly in the order of magnitude of 0.1 m/s. This is the systematical uncertainty caused by the measurement system and explained before. And Fig 8 shows that the RPA was not able to measure small vertical wind speeds adequately. Considering this, what insights are left?*

Response : We attempt to clarify in the manuscript, 1) that the lower limit of measuring vertical wind is 0.1 m/s which is largely sufficient for aerosol-cloud interaction studies, and 2) measurements of the wind-RPA and the cloud radar do not sample the same air mass, so agreement within 0.1 m/s implies that both observing systems (cloud radar and RPA) measure the same state of the boundary layer. The insight of this work lies in the ability of the RPA to identify different states of the boundary layer (in/out of cloud, over water/land), and to provide a range of vertical wind velocities near cloud base to accurately determine the number of aerosol particles that activate into cloud droplets.

** 11/28 The abstract says 'are now able to accurately measure ... even in clouds'. But now it is written that water is accumulated within the probe, making it useless. It seems (what could be expected) that 5-hole probes cannot be used in clouds, can they?*

Response : Yes, in fact, the 5-hole probe can be used in clouds – we clearly show this in the comparison with the cloud radar at Mace Head. We agree that the probe can be improved, and we are addressing this issue.

** 14/17 'Motions induced ...' Well, this can be expected in case the wind was properly calculated using the correct formulas!*

Response : We have addressed this issue in response 5/4.

** 14/19 My suspicion: the simplified wind equations (that possibly hold for large and heavy aircraft) and the faulty calibration caused all the insufficient agreements between the RPA data and other data and theory.*

Response : As it has been addressed in the previous responses, the linear approximation for the calibration coefficients and the simplified wind equations do not affect the results as we operated the RPA within the quasi-linear response regime of the probe, on straight-and-level legs.

** 14/24 'following Kolmogorov' - actually, not really. See above.*

Response : We have addressed this issue in response Section 4.1, in Fig.6.

**14/25 Considering that the Kolmogorov distribution was not measured, I doubt that any isotropy of the turbulent flow can be assumed. Can you prove that the variances of the two horizontal wind components are equal, as written in the text?*

Response : Perhaps it is not clear, but we invite the reviewer to take a closer look at Fig.9 in the manuscript, which compares the variances of the horizontal wind components from the sonic anemometers at different heights. The results show that the isotropy assumption is a better approximation at 60 m.agl compared to 30 m.agl. We show these results to support the arguments for improving the calculation of TKE and because data from the mast at 60 m.agl was not always available for comparison to the RPA.

** 14/27 This is not surprising. Without a proper heading you cannot measure the wind vector. How accurate was the heading so far?*

Response : Of course, drift in heading is a known issue for INS. The calibration of the magnetometer helps; however, its time response is relatively slow. Reineman et al. (2013) and Thomas et al. (2012) address this issue with state-of-the-art INS that are much more precise (as well as expensive and heavy). INS technology continues to evolve, and as stated in the conclusions, we are addressing these issues by incorporating an INS with a differential GPS system.

## Technical corrections

** Proper use of hyphen! E.g. line 3 on page 2: 'boundary-layer turbulence' would be correct. Also correct would be (in contrast), again in line 3 on page 2: 'aircraft based wind measurements'.*

Response: We updated the text.

** Language has to be improved, e.g. in line 2 on page 2: 'vectors are an essential parameter' - this doesn't make sense.*

Response : The manuscript has been updated.

In the manuscript 2/1 : "Vertical wind is a key parameter for understanding aerosol-cloud interactions."

** Using the cross 'x' in equations is usually reserved for the vector product, not for normal scalar multiplication.*

Response : The cross 'x' has been removed from equations to avoid any confusion.

Response to anonymous referee #2

## General comments

We thank the reviewer for his comments. The manuscript has been restructured in order to address the reviewers' concerns. The main modifications are the calibration of the 5-hole probe, the use of full wind equations instead of simplified equations (Lenschow et al., 1989), and a more detailed analysis of the PSDs to understand the origin of differences between the RPA and mast measurements. We also show that difference in vertical wind distributions does not deeply affect the calculation of cloud droplet number for aerosol-cloud study.

## Specific comments

Comments from the reviewer appear in italic, response from the authors follows. As the manuscript has been mainly rewritten, we invite the reviewers to directly refer to the updated version of the manuscript for specified sections.

**The manuscript is confusing at times, and will require a careful rewrite to be suitable for publication.*

Response: We have reworked the manuscript to clarify the sections, in particular related to the calibration and the validation of the results with sonic anemometers.

**The spectral levels, "spikes" and slopes found in the frequency spectra off the three components of the motion compensated winds computed from the RPAS (and compared against the anemometer ground truth) shown in figure 7 are very concerning and not discuss in depth in the text.*

Response: The Power Spectral Density (PSD) functions have been updated. The analysis now uses the Welch's method to calculate PSDs. The spikes have been suspected to originate from the INS. We agree that there are still issues to address turbulence or fluxes measurements (particularly calculations of divergence and convergence), as these studies require highly accurate wind measurements. However, for the purpose of aerosol-cloud interaction study, the accuracy of the updraft measurements conducted in the present work has been shown to be sufficient (Section 6).

**I went back to Reineman et al. 2013, there found slight spectral level differences for the lowest wavenumbers, but nothing as significant as what is presented here.*

Response: We thank the reviewer for pointing this statement out. There is actually a good agreement in spectral level for vertical wind in Reineman et al. (2013). However, a difference of level of spectral energy for the vertical wind component is found in Reuder et al. (2016) and Båserud et al. (2016) for the SUMO RPA compared to sonic anemometer. The TKE measurements from the $M^2AV$ in Lampert et al. (2016) is higher than TKE from sonic anemometer on a mast during the afternoon and the night, which also implies higher energy levels of the PSDs. The manuscript has been updated to assess the source of difference in PSDs between the RPA and the mast. We found higher energy in ground speeds provided by the INS for frequencies lower than 0.3 Hz, which influence the wind calculation.

*I would encourage the authors to go back to the data processing and ensure the algorithm is motion compensating the relative winds computed from the 5-hole probe correctly.*

Response: The calibration of the 5-hole probe has been updated, using polynomial instead of linear coefficients for $\alpha$ the angle of attack and $\beta$ the angle of sideslip. Polynomial coefficients from Treaster et al. (1978) method have been determined for static and dynamic pressures, and then used in the calculation of $V_a$ the airspeed. As the RPA operates in the quasi-linear regime of the 5-hole probe (pitch and roll angles < 10 deg), no significant modification of the wind results has been observed with the updated calibration. The full wind equations have been used instead of the simplified equations (Lenschow et al., 1989). A comparison between the wind results has been conducted to show a difference less than $0.03 \pm 0.05$ m/s on straight-and-level legs. However, to avoid any confusion, the full wind equations have been employed in the analysis, except when specified (uncertainty analysis on $w$, section 3.2).

*Figure 8 further demonstrates the disagreement between the sonic and RPAS wind measurements.*

Response: We disagree; actually, Figure 8 shows agreement. Uncertainty at low wind speeds related to noise – and the peak at near zero-winds is expected. The limit of detection is $\pm$ 0.1 m/s (also quantified in Figure 5), which is largely sufficient for studying aerosol-cloud interactions. In the manuscript, a section has been added to quantify the influence of the updraft in term of cloud droplet number concentrations.

# Bibliography


Anderson, J.D. (2001). *Fundamentals of Aerodynamics, third edition*. 1128 pp, ISBN13: 978-0071289085. McGraw-Hill.

Båserud, L. et al. (2016). "Proof of concept for turbulence measurements with the RPAS SUMO during the BLLAST campaign". In: *Atmospheric Measurement Techniques* 9.10, pp. 4901–4913. DOI: 10.5194/amt-9-4901-2016.

Bohn, D. and H. Simon (1975). "ehrparametrige Approximation der Eichräume und Eichflächen von Unterschall- bzw. Überschall-5-Loch-Sonden. tm". In: *Technisches Messen*, pp. 81–89. DOI: 10.1524/teme.1975.468479.jg.81.

Boiffier, J.L (1998). *The dynamics of flight, the equations*. ISBN 0 471 94237 5. John Wiley and Sons.

Canut, G. et al. (2016). "Turbulence fluxes and variances measured with a sonic anemometer mounted on a tethered balloon". In: *Atmospheric Measurement Techniques* 9.9, pp. 4375–4386. DOI: 10.5194/amt-9-4375-2016.

Crawford, Timothy L. and Ronald J. Dobosy (1992). "A sensitive fast-response probe to measure turbulence and heat flux from any airplane". In: *Boundary-Layer Meteorology* 59.3, pp. 257–278. ISSN: 1573-1472. DOI: 10.1007/BF00119816.

Elston, Jack et al. (2015). "Overview of Small Fixed-Wing Unmanned Aircraft for Meteorological Sampling". In: *Journal of Atmospheric and Oceanic Technology* 32.1, pp. 97–115. DOI: 10.1175/JTECH-D-13-00236.1. eprint: https://doi.org/10.1175/JTECH-D-13-00236.1.

Garman, K. E. et al. (2006). "An Airborne and Wind Tunnel Evaluation of a Wind Turbulence Measurement System for Aircraft-Based Flux Measurements". In: *Journal of Atmospheric and Oceanic Technology* 23.12, pp. 1696–1708. DOI: 10.1175/JTECH1940.1. eprint: https://doi.org/10.1175/JTECH1940.1.

Kroonenberg, Aline Van Den et al. (2008). "Measuring the Wind Vector Using the Autonomous Mini Aerial Vehicle M2AV". In: *Journal of Atmospheric and Oceanic Technology* 25.11, pp. 1969–1982. DOI: 10.1175/2008JTECHA1114.1. eprint: https://doi.org/10.1175/2008JTECHA1114.1.

Lampert, A. et al. (2016). "A study of local turbulence and anisotropy during the afternoon and evening transition with an unmanned aerial system and mesoscale simulation". In: *Atmospheric Chemistry and Physics* 16.12, pp. 8009–8021. DOI: 10.5194/acp-16-8009-2016.

Lenschow, D.H. and P. Spyers-Duran (1989). "Measurement Techniques : Air motion sensing". In: *National Center for Atmospheric Research, Bulletin No.23*. URL: https://www.eol.ucar.edu/raf/Bulletins/bulletin23.html.

Reineman, Benjamin D. et al. (2013). "Development and Testing of Instrumentation for UAV-Based Flux Measurements within Terrestrial and Marine Atmospheric Boundary Layers". In: *Journal of Atmospheric and Oceanic Technology* 30.7, pp. 1295–1319. DOI: 10.1175/JTECH-D-12-00176.1. eprint: https://doi.org/10.1175/JTECH-D-12-00176.1.

Reuder, J et al. (2008). "SUMO: A small unmanned meteorological observer for atmospheric boundary layer research". In: *IOP Conference Series: Earth and Environmental Science* 1.1, p. 012014. DOI: 10.1088/1755-1307/1/1/012014.

Reuder, J. et al. (2016). "Exploring the potential of the RPA system SUMO for multipurpose boundary-layer missions during the BLLAST campaign". In: *Atmospheric Measurement Techniques* 9.6, pp. 2675–2688. DOI: 10.5194/amt-9-2675-2016.

Reuder, Joachim et al. (2012). "FLOHOF 2007: an overview of the mesoscale meteorological field campaign at Hofsjökull, Central Iceland". In: *Meteorology and Atmospheric Physics* 116.1, pp. 1–13. ISSN: 1436-5065. DOI: 10.1007/s00703-010-0118-.

Sanchez, K.J. et al. (2017). "Top-down and bottom-up aerosol-cloud-closure: towards understanding sources of uncertainty in deriving cloud radiative forcing". In: *Atmos. Chem. Phy.* DOI: 10.5194/acp-2017-201,2017.

Spiess, Thomas et al. (2007). "First application of the meteorological Mini-UAV 'M2AV'". In: *Meteorologische Zeitschrift* 16.2, pp. 159–169. DOI: 10.1127/0941-2948/2007/0195.

Thomas, R. M. et al. (2012). "Measurement of turbulent water vapor fluxes using a lightweight unmanned aerial vehicle system". In: *Atmospheric Measurement Techniques* 5.1, pp. 243–257. DOI: 10.5194/amt-5-243-2012.

Treaster, A. L. and A. M. Yocum (1978). "The calibration and application of five-hole probes". In: *NASA STI/Recon Technical Report N* 78.

Truong, S. S. (2011). "Conical Probe Calibration and Wind Tunnel Data Analysis of the Channeled Centerbody Inlet Experiment". In: URL: http://digitalcommons.calpoly.edu/aerosp/44.

Wildmann, N., S. Ravi, and J. Bange (2014). "Towards higher accuracy and better frequency response with standard multi-hole probes in turbulence measurement with remotely piloted aircraft (RPA)". In: *Atmospheric Measurement Techniques* 7.4, pp. 1027–1041. DOI: 10.5194/amt-7-1027-2014.

# Vertical Wind Velocity Measurements using a 5-hole Probe with Remotely Piloted Aircraft to Study Aerosol-Cloud Interactions

Radiance Calmer[1], Greg Roberts[1,2], Jana Preissler[3], Kevin Sanchez[1,2], Solène Derrien[4], and Colin O'Dowd[3]

[1]CNRM UMR 3589, Météo-France/CNRS,Toulouse, France;
[2]Scripps Institution of Oceanography, University of California, San Diego, CA;
[3]School of Physics and Centre for Climate and Air Pollution Studies, National University of Ireland Galway, Ireland;
[4]Laboratoire d'Aérologie, University of Toulouse, CNRS, France

*Correspondence to:* Radiance Calmer (radiance.calmer@meteo.fr)

Submission to Atmospheric Measurement Techniques journal

**Abstract.** The importance of vertical wind velocities (in particular positive vertical wind velocities or updrafts) in atmospheric science has motivated the need to deploy multi-hole probes developed for manned aircraft in small Remotely Piloted Aircraft (RPA). In atmospheric research, lightweight RPAs ($<$ 2.5 kg) are now able to accurately measure atmospheric wind vectors, even in a cloud, which provides essential observing tools for understanding aerosol-cloud interactions. The European project BACCHUS (impact of Biogenic versus Anthropogenic emissions on Clouds and Climate: towards a Holistic UnderStanding) focuses on these specific interactions. In particular, vertical wind velocity at cloud base is a key parameter for studying aerosol-cloud interactions. To measure the three components of wind, a RPA is equipped with a 5-hole probe, pressure sensors, and an Inertial Navigation System (INS). The 5-hole probe is calibrated on a multi-axis platform, and the probe/INS system is validated in a wind tunnel. Once mounted on a RPA, power spectral density (PSD) functions and turbulent kinetic energy (TKE) derived from the 5-hole probe are compared with sonic anemometers on a meteorological mast. During a BACCHUS field campaign at Mace Head Atmospheric Research Station (Ireland), a fleet of RPAs was deployed to profile the atmosphere and complement ground-based and satellite observations of physical and chemical properties of aerosols, clouds and meteorological state parameters. The 5-hole probe was flown on straight-and-level legs to measure vertical wind velocities within clouds. The vertical velocity measurements from the RPA are validated with vertical velocities derived from a ground-based cloud radar by showing that both measurements yield model-simulated cloud droplet number concentrations within 10 %. The updraft velocity distributions illustrate distinct relationships between vertical cloud fields in different meteorological conditions.

## 1 Introduction

Vertical wind is a key parameter for understanding aerosol-cloud interactions. In tracing the evolution of aircraft-based wind measurements in the atmosphere, three axes of development have been pursued since the 1960s: improvements in airborne platforms, inertial navigation systems (INS) and sensors. Airborne platforms have evolved from large aircraft (e.g., Canberra PR3, Axford (1968) or NCAR Queen Air, Brown et al. (1983)) to ultra-light unmanned aerial systems (e.g., M$^2$AV; Spiess et al. (2007)). INS measure linear and rotational motion of the aircraft (or unmanned aerial system) and are used to back out wind vectors in the Earth's coordinate system. A major improvement in INS was the integration of GPS (Global Positioning System) data with fusion sensors (Khelif et al., 1999). The overall accuracy of atmospheric wind vectors has improved drastically, from 1 m s$^{-1}$ with wind vanes (Lenschow and Spyers-Duran, 1989) to 0.03 m s$^{-1}$ with a multi-hole probe and state-of-the-art INS (Garman et al., 2006). Over the past decade, GPS, INS and sensors have become sufficiently miniaturized to be deployed on ultralight remotely piloted aircraft systems (RPAS)[1], which has extended observational capabilities previously limited to traditional manned aircraft.

A wide range of remotely piloted aircraft (RPA)[2] has been used to measure atmospheric winds, from a 600 g SUMO (Reuder et al., 2012) to a 30 kg Manta (Thomas et al., 2012). In particular, a multi-hole probe paired with an INS has been the main mechanism for obtaining vertical winds in fixed-wing RPA. Ultimately, the combination of the multi-hole probe, pressure sensors, and the INS dictates the precision of atmospheric wind measurements. The following accuracies for vertical wind measurements $w$ were reported in the literature for different RPA platforms; they were obtained by different methods, which provided either 1-sigma uncertainty or systematic error analysis associated with a specific pair of probe/INS. In van den Kroonenberg et al. (2008), a custom 5-hole probe on the M$^2$AV, implemented with a GPS-MEMS-IMU was reported with an accuracy for $w$ within $\pm$ 0.5 m s$^{-1}$. The accuracy was based on a systematic error estimation using characteristic flight parameters with a reference state of $w$ = 1 m s$^{-1}$. The uncertainty in $w$ reported for the SUMO (Reuder et al., 2016) is $\pm$ 0.1 m s$^{-1}$ as given by the manufacturer (Aeroprobe Corporation); however, the impact of the INS was not included in their analysis. In Thomas et al. (2012), the Manta RPA was also equipped with a commercial Aeroprobe and a C-Migits-III INS to obtain a minimum resolvable $w$ of 0.17 m s$^{-1}$ (1-sigma). The uncertainty analysis was based on a Gaussian error propagation described in Garman et al. (2006). The Manta and ScanEagle RPAs described in Reineman et al. (2013) achieved precise wind measurements with a custom 9-hole probe and NovAtel INS with reported uncertainties for $w$ within $\pm$ 0.021 m s$^{-1}$. Their uncertainty was obtained from a Monte-Carlo simulation, and was also consistent with reverse-heading maneuvers. The higher precision reported in the latter study (Reineman et al., 2013) is related to probe design and the high precision of the INS. The vertical wind measurements in Reineman et al. (2013) have a similar performance as reported with the BAT probe ("Best Air Turbulence Probe") on a small piloted aircraft (Garman et al., 2006). For aerosol-cloud studies, vertical wind measurements near 0.1 m s$^{-1}$ are needed, which is within instrument uncertainties for most of the systems described above.

[1] Commonly called unmanned aerial vehicle (UAV)

[2] RPA refers to the aircraft, as RPAS represents the airframe and the ground control station

Elston et al. (2015) has identified four main points that still need to be addressed for atmospheric wind measurements using RPAS: (1) true heading remains one of the main sources of inaccuracy in horizontal wind calculation; (2) precise altitude measurement with GPS impacts vertical wind calculations; (3) miniaturization of INS for small RPA with better accuracy of fusion sensors; and (5) RPAS regulations and integration in the airspace, which delay research progress.

Until recently, wind measurements from RPA have been mainly used for atmospheric boundary layer studies of turbulence and atmospheric fluxes. In the BLLAST field campaign, multiple RPAs have been deployed to study the evolution of the boundary layer during the transition between afternoon and evening periods (Lothon et al., 2014). Results of sensible and latent heat fluxes, and also turbulent kinetic energy (TKE), were calculated from the SUMO RPA flights, (Reuder et al. (2016); Båserud et al. (2016)). The operation of the $M^2AV$ and the MASC RPAs during the BLLAST campaign was described in Lampert et al. (2016) with a particular focus on turbulence. A comparison of nearly co-located measurements of TKE between different platforms (tethered balloon, RPA, and manned aircraft) compared the different techniques of obtaining atmospheric wind vectors (Canut et al., 2016).

In addition, vertical winds are used to study aerosol-cloud interactions (ACI), which is the focus of the collaborative project, BACCHUS (impact of Biogenic versus Anthropogenic emissions on Clouds and Climate : towards a Holistic UnderStanding) (BACCHUS, 2016). One critical parameter in ACI studies, not previously measured by RPA, is the vertical wind velocity $w$ at cloud base. Peng et al. (2005) show the importance of measuring vertical velocity in convective clouds for aerosol-cloud closure studies, and highlight the need for more cloud microphysical data to further test the sensitivity of cloud droplet number concentration to variations in vertical velocity. Sullivan et al. (2016) investigate the role of updraft velocity in temporal variability of clouds in global climate models (GCMs), and emphasize that simulated vertical velocity distributions are too rarely compared to observations, citing the lack of data. As more than half of the temporal variability in droplet number was due to updraft velocity fluctuations, Sullivan et al. (2016) call for coordinated effort in the atmospheric science community to address the current gap in observations, otherwise uncertainties in modeled cloud droplet number and subsequent radiative properties may remain irreducible. In Conant et al. (2004) and Sanchez et al. (2017), updraft velocity has also been described as a critical parameter, along with cloud condensation nuclei (CCN) spectra, to derive cloud droplet number in ACI studies. Both of these studies show that cloud microphysical and radiative properties are well simulated when CCN spectra and cloud updrafts have been measured.

Therefore, the motivation of the present work is driven by the need for vertical wind measurements to better quantify ACI. Commercial multi-hole probes do exist (i.e., Aeroprobe Corporation and Vectoflow); however, pressure sensor measurements and integration of the INS have been developed for this study; hence, the need to calibrate and validate the probe/INS pair. Section 2 of the manuscript describes the RPA platform and the methods used to calculate atmospheric wind vectors. Section 3 presents the calibration of a commercial 5-hole probe and its custom electronics in a wind tunnel, complemented by an uncertainty analysis on vertical wind velocity, $w$. Section 4 shows a comparison of the 5-hole probe on a RPA with sonic

anemometers on a meteorological mast. Vertical wind velocities from the RPA are compared to those of a cloud radar in different meteorological conditions (Section 5). Lastly, the sensitivity of cloud droplet number is investigated as a function of updraft distributions (Section 6).

## 2 Materials and methods

### 2.1 Remotely Piloted Aircraft (RPA) description

The RPAs used here to measure vertical wind velocity and study aerosol-cloud interactions are based on the commercially available Skywalker X6 model. The wingspan is 1.5 m long, and take-off weight varies between 1.5 kg and 2.5 kg depending on the mission specific payload. The RPA's autonomous navigation system is the open source autopilot Paparazzi from Ecole Nationale de l'Aviation Civile (Brisset et al., 2006). One of the RPAs (wind-RPA) is specially equipped to measure atmospheric wind vectors, particularly vertical wind, whose validation and study of different cloud cases is the purpose of this work. Its take-off weight is 1.5 kg with a 500 g payload. The cruise airspeed is approximately 16 m $s^{-1}$.

### 2.2 Payload instrumentation

Wind vectors are obtained from a 5-hole probe (Aeroprobe Corporation) linked to its differential pressure sensors (All Sensors) by flexible tubing, and an INS (Lord Sensing Microstrain 3DM-GX4-45). The data from both the INS and the pressure sensors are recorded by the same acquisition system to ensure precise synchronization. The acquisition frequency is 30 Hz, and data are averaged to 10 Hz for analysis. The 5-hole probe consists of a 6 mm diameter stainless tube with a hemi-spherical tip (Fig.1). The associated electronics have been designed at the Centre National de Recherches Météorologiques (CNRM), and consist of three differential pressure sensors (All-Sensors 5inch-D1-MV) and one absolute pressure sensor (All Sensors MLV-015A). The configuration of pressure sensor connections are similar to Reineman et al. (2013). The tubing length between the probe manifold and the pressure sensors is less than 15 cm and the inner diameter is 0.1 mm. These dimensions are also similar to Wildmann et al. (2014), where an extensive study of tubing issues is conducted. Figure 1a illustrates the probe schematic: hole 1 measures the pressure at the stagnation point of the tip; the differential pressure between holes 2 and 3 provides $\beta$, the angle of sideslip; the differential pressure between 4 and 5 gives $\alpha$, the angle of attack; and hole 6, a ring around the probe, corresponds to the static pressure port. The airspeed, $V_a$, is calculated from the dynamic and static pressure (holes 1 and 6). To obtain atmospheric winds, the 5-hole probe system must be calibrated in the probe's coordinate system and converted to the Earth's coordinate system. The INS sends information obtained by an extended Kalman filter to the data acquisition system regarding attitude angles, roll $\phi$, yaw $\psi$ and pitch $\theta$, GPS time and GPS position and altitude, and ground speeds of the RPA in Earth's coordinate system. Schematics of coordinate systems and angles are shown in Fig.1b. The payload of the wind-RPA also includes temperature (IST, Model P1K0.161.6W.Y.010), absolute pressure (All Sensors, Model 15PSI-A-HGRADE-SMINI) and relative humidity sensors (IST, P14 Rapid-W). Two Licor LI-200R pyranometers (400 to 1100 nm

wavelengths) are installed on the fuselage; one facing up to measure downwelling solar irradiance, and the other facing down to measure upwelling solar irradiance. The ratio of the downwelling and upwelling solar irradiance is used to detect the presence of cloud (when this ratio approaches unity).

### 2.3 Methods

Atmospheric wind vectors in the Earth's coordinate system are obtained by subtracting the measured motion of the RPA (given by the INS), from the motion of the air (given by the 5-hole probe), as stated in Lenschow and Spyers-Duran (1989). The angle of attack $\alpha$, the angle of sideslip $\beta$, and the airspeed $V_a$ are measured by the 5-hole probe in the probe coordinate system and then transformed to the RPA coordinate system; while the attitude angles from the INS provide the transformation of $\alpha$, $\beta$ and $V_a$ from the RPA coordinate system to the Earth's coordinate system. Lenschow equations (Lenschow and Spyers-Duran, 1989) are therefore followed to derive the atmospheric wind vectors in the Earth's coordinate system. The angular acceleration of the RPA is negligible, particularly during straight-and-level legs because the distance between the 5-hole probe and the INS is on the order of centimeters. More details on wind equations, and schematics of coordinate systems are found in Lenschow and Spyers-Duran (1989), Boiffier (1998), and van den Kroonenberg et al. (2008). The calibration of the 5-hole probe has been performed in a wind tunnel (Theodor Friedrichs & Co) with a diameter of 70 cm. The uncertainty associated with the wind velocity in the wind tunnel is less than 2 %.

## 3 Calibration of the 5-hole probe

The calibration of the 5-hole probe is based on a method described in Wildmann et al. (2014), and consists of a series of wind tunnel experiments to characterize the response of the 5-hole probe at different angles. The 5-hole probe, the pressure sensors, and the INS are installed in the wind tunnel on a two-axis platform with motion in vertical and horizontal planes (Fig.2). The calibration of the 5-hole probe is a two-step process — first calibrating the differential pressure sensors (mbar), then associating the differential pressures in mbar to angles ($\alpha$ and $\beta$; degrees) and airspeed ($V_a$; m s$^{-1}$). The two-axis platform rotates in the pitch axis (motion in the vertical plane) and yaw axis (motion in the horizontal plane), controlled with a LabView program (Fig.2). The amplitude of pitch and yaw angles varies up to $\pm$ 15 deg to simulate the largest envelope of expected flight conditions. In the wind tunnel, the angle of attack $\alpha$ (5-hole probe) and the pitch angle $\theta$ (INS) are, by definition, the same for a well-aligned system; as for the angle of sideslip $\beta$ (5-hole probe) and the yaw angle $\psi$ (INS). The INS is used as a reference angle measurement between the 5-hole probe and the airflow in the wind tunnel. The determination of $\alpha$, $\beta$, and $V_a$ from the 5-hole probe depends on four coefficients $C_\alpha$, $C_\beta$, $C_q$ for the dynamic pressure, and $C_s$ for the static pressure (Wildmann et al. (2014); Treaster and Yocum (1978)). To account for offsets in the alignment between the 5-hole probe, INS and wind tunnel, experiments are performed with the probe in the standard orientation shown in Fig.1, with roll angle equal to 0 deg (+ markers in Fig.3), and the probe in inverted orientation for the roll angle equal to 180 deg (x markers in Fig.3). Likewise, the same procedure is followed by rotating the 5-hole probe by $\pm$ 90 deg to determine the offset in the horizontal plane for $\beta$. INS angles and ratios of differential pressure sensors are recorded for platform positions between $\pm$ 15

deg for three airspeeds in the wind tunnel. Figure 3 shows that calibration coefficients are within instrument uncertainty for airspeed between 15 and 25 m s$^{-1}$, and the calibration shows a nearly linear relationship when the probe is within $\pm$ 10 deg. A systematic offset of 7 % has been found between the calculation of $V_a$ (5-hole probe) and the wind tunnel airspeed. The 1-$\sigma$ uncertainty in $V_a$ determined by the 5-hole probe is 0.1 m s$^{-1}$.

To extend the measurements beyond the single-axis of motion described previously, the pitch and yaw angles of the two-axis platform are varied concurrently (Fig.4a), and the corresponding differential pressure coefficients $C_\alpha$ and $C_\beta$ are measured (Fig.4b). This yields a matrix relating the probe's response to the relative vertical ($\alpha$) and horizontal ($\beta$) winds (Fig.4). The grid in Fig.4a illustrates the discrete 5 deg steps in pitch and yaw angles to create a 5x5 calibration matrix for a constant wind speed of 15 m s$^{-1}$. Similar results are also shown in Wildmann et al. (2014). The horizontal angular bias in Fig.4 is due to a 3 deg roll angle in the mounting of the two-axis platform in the wind tunnel. The asymmetry in the calibration matrix (i.e., higher degree of non-linearity on the right side of Fig.4b) results from a discrepancy in the alignment of the 5-hole probe relative to the wind tunnel air flow. The offset between the two-axis platform and the INS is also visible as the grid in Fig.4a is not centered on 0 (also called the zero-angle offset). The calibration coefficients show a nearly linear relationship for $C_\alpha$ and $C_\beta$ between values of $\pm$ 0.7, which corresponds to $\alpha$ and $\beta$ within $\pm$ 10 deg (Fig.4).

### 3.1 Experimental error analysis on vertical wind velocity

The performance of the 5-hole probe/INS pair is verified by using a dynamic platform to generate motion in the controlled environment of the wind tunnel. The wind tunnel provides a laminar flow, thus vertical wind velocity is, by definition, zero even when the two-axis platform is in motion. Therefore, the response of the 5-hole probe can be validated in the wind tunnel by controlling the amplitude (up to $\pm$ 15 deg) and the angular rate of change (up to 22 deg s$^{-1}$) of the platform in the vertical (pitch) axis. As expected, the estimates of vertical wind velocity, $w$, in the wind tunnel are close to zero. The 1-$\sigma$ standard deviation of $w$ increases with the angular rate of change of the platform (Fig.5), which seems to be related to a lag in the INS's Kalman filtering process. Under the flight conditions reported in this work, the pitch angle rate of change rarely exceeds $\pm$ 10 deg s$^{-1}$ during straight-and-level legs, implying the minimum resolution of vertical wind velocity measurement with the 5-hole probe/INS system is 0.07 m s$^{-1}$. The uncertainties in $w$ increase when accounting for all parameters, as shown in the next section.

### 3.2 Gaussian error propagation on vertical wind velocity

To measure vertical wind velocity of a cloud field, the RPA flies straight-and-level legs at a prescribed altitude. Results from such flight legs show that pitch and roll angles are almost always less than 10 deg with a rate of change within $\pm$ 10 deg s$^{-1}$, as mentioned in the previous section. In such conditions, the 5-hole probe response lies in the quasi-linear regime of the calibration coefficients (Fig.4), and the small-angle approximations accurately represent the full set of wind equations

(Lenschow and Spyers-Duran, 1989). Therefore, the small-angle approximation for the vertical wind velocity equation is used to conduct an uncertainty analysis on $w$ :

$$w = -V_a \sin(\theta - \alpha) + V_z \tag{1}$$

with $V_a$ the airspeed, $\theta$ the pitch angle, $\alpha$ the angle of attack, and $V_z$ the vertical RPA speed. The method used to determine the Gaussian error propagation is similar to the uncertainty analysis conducted in Garman et al. (2006). Here, we present the contribution of each component in Equation 1 (i.e., angle of attack, airspeed, pitch, and vertical RPA speed) to the uncertainty in $w$. The 1-sigma uncertainty related to the vertical wind velocity is:

$$\sigma_w = \sqrt{\left(\frac{\partial w}{\partial \alpha}\sigma_\alpha\right)^2 + \left(\frac{\partial w}{\partial V_a}\sigma_{V_a}\right)^2 + \left(\frac{\partial w}{\partial \theta}\sigma_\theta\right)^2 + \left(\frac{\partial w}{\partial V_z}\sigma_{V_z}\right)^2} \tag{2}$$

where $\sigma_{V_a}$ is 0.1 m s$^{-1}$ (from wind tunnel measurements), $\sigma_\theta$ is 0.25 deg and $\sigma_{V_z}$ is 0.1 m s$^{-1}$ (both provided by the INS manufacturer). The uncertainties are summarized in Table 1. The error propagation is conducted for $\alpha$ based on $C_\alpha$ in the linear regime (with the slope $a_\alpha$ and the intersect $b_\alpha$) :

$$\alpha = a_\alpha C_\alpha + b_\alpha \quad \text{and} \quad C_\alpha = \frac{\Delta(P_4 - P_5)}{\Delta(P_1 - P_6) - \Delta P} \tag{3}$$

With $\Delta P = \frac{1}{4}(|\Delta(P_4 - P_5)| + |\Delta(P_2 - P_3)|)$, $\Delta(P_4 - P_5)$ the differential pressure between holes 4 and 5, $\Delta(P_2 - P_3)$ the differential pressure between holes 2 and 3, and $\Delta(P_1 - P_6)$ the differential pressure between holes 1 and 6 (Fig.1a). Error propagation of Equation 3 leads to:

$$\sigma_\alpha = a_\alpha \sigma_{C_\alpha} \tag{4}$$

and, as $C_\alpha$ is calculated based on the differential pressures measured by the 5-hole probe :

$$\sigma_{C_\alpha} = \sqrt{\left(\frac{\partial C_\alpha}{\partial \Delta(P_4 - P_5)}\sigma_{\Delta(P_4-P_5)}\right)^2 + \left(\frac{\partial C_\alpha}{\partial \Delta(P_2 - P_3)}\sigma_{\Delta(P_2-P_3)}\right)^2 + \left(\frac{\partial C_\alpha}{\partial \Delta(P_1 - P_6)}\sigma_{\Delta(P_1-P_6)}\right)^2} \tag{5}$$

The analysis presented here results in $\sigma_w$ = 0.12 m s$^{-1}$, which is similar to the uncertainty in $w$ based on the wind tunnel measurements (from Section 3.1) and comparable to the results reported by other studies cited in the introduction.

## 4 Comparison of vertical winds from RPA and sonic anemometers

The measurements of vertical wind velocity on an RPA were compared to sonic anemometers (Campbell CSAT3 3-D Sonic Anemometer) under calm wind conditions at Centre de Recherches Atmosphériques (CRA), which is an instrumented site of the Pyrenean Platform of Observation of the Atmosphere (P2OA), near Lannemezan, France. The purpose of the comparison is 1) to assess the performance of the RPA measurement of updraft by comparing Power Spectral Density (PSD) and vertical wind $w$ distributions measured by sonic anemometers, and 2) to calculate turbulent kinetic energy (TKE) used to study boundary layer dynamics and compare with previous studies. Table 2 summarizes flight and wind conditions encountered during these validation experiments. The sonic anemometers are installed on a meteorological mast at 30 m.agl (meters above ground level) and 60 m.agl as part of permanent installations at the CRA. During the experiment, the RPA flew straight N-S and E-W legs in the vicinity of the mast at 60 m.agl. The leg length was 1600 m and the duration of flights was approximately 1.5 hours. A total of five flights were conducted in different meteorological conditions: a series of three flights were conducted on 15 October 2015 at different times of the day, one flight was conducted in the morning on 20 May 2016, and the last flight was conducted in the afternoon on 7 July 2016 (Table 2). While all flights were conducted in low wind conditions (wind speed less than 4 m $s^{-1}$), the turbulent conditions differed from one flight to another. The roll angle exceeded 10 deg less than 1 % of the time, except during Flight 4 when roll exceeded 10 deg 2 % of the time. The pitch angle never exceeded 10 deg, except when approaching stall speed and, even then, only exceeded 10 deg less than 0.1 % of the time.

### 4.1 Power spectral density functions

To assess the performance of the RPA measurements of atmospheric wind, PSD functions for each of the three wind components of the RPA are compared to PSDs from sonic anemometers. The PSDs of the wind velocities from RPA and sonic anemometers generally follow the -5/3 slope from the Kolmogorov law as expected (Fig.6). The PSDs for Flights 1, 2, and 3 are averaged to illustrate the probe/INS performance prior to a magnetometer calibration and revised Kalman filtering of the INS (Flight 5). During Flight 4, the RPA experienced excess motion due to an airspeed close to stall speed, which degraded the wind measurements, consequently, results from Flight 4 are not included in the analysis. For Flights 1, 2, and 3 (prior to reconfiguring the INS), discrepancies in the PSD energy level are visible at $10^{-1}$Hz particularly on the $u$-component (Fig.6b). The bump in the $u$-component at $10^{-1}$ Hz is related to the uncertainty in the INS heading measurement, which impacts the horizontal wind calculation, particularly, the transversal wind component (the wind component perpendicular to RPA heading). Based on the reverse-heading maneuvers, the uncertainty in horizontal winds is estimated to be within $\pm$ 1.1 m $s^{-1}$. After reconfiguring the INS, a notable improvement in PSDs of all three wind components (particularly $u$-component; transversal wind) was observed (Fig.6; blue lines). The improvement in INS performance clearly demonstrates the importance of precise INS filtering and heading measurements.

Nonetheless, the PSDs still show a systematic difference between the energy levels related to wind components from the sonic anemometer and the RPA. For the three wind components calculated from RPA measurements, the energy level of ground speeds obtained from the INS ($V_x$, $V_y$, and $V_z$) are higher than the other terms in wind equations for frequencies less than 0.3 Hz. To assess the origin of the different energy levels, the decomposition of the vertical wind equation $w$ (Lenschow and Spyers-Duran, 1989) is based on the simplified form shown as Equation 1. PSDs of each component of $w$, $V_z$ (vertical ground speed) and $A_w$ (defined as $-V_a \sin(\theta - \alpha)$), are calculated to assess biases related to the INS (Earth frame) and the 5-hole probe (RPA frame). The average results from the RPA flights and the sonic anemometers are presented in Fig.7. The high energy levels at low frequencies seem to be related to uncertainties (even a drift) associated with the vertical velocity measurement. The higher energy levels do translate to systematically higher TKE values (Section 4.2); however, these concerns do not significantly impact the results in aerosol-cloud interaction studies (Section 6).

The relatively high energy levels associated with the PSDs are not unique; yet, it has not been adequately explained in the literature. Båserud et al. (2016) and Reuder et al. (2016) reported systematically high energy levels of the vertical wind component from the SUMO compared to sonic anemometers on a mast (also at CRA in Lannemezan, France). The issue of higher energy levels was then to "be further investigated in the future." Other studies have compared turbulent kinetic energy (TKE) values between RPA platforms and a reference; the TKE is linked to PSD energy levels via the variance of each wind component. For example, Lampert et al. (2016) compare TKE between 5-hole probe on the $M^2AV$ and sonic anemometers (also on the mast at CRA, Lannemezan) and show higher TKE values associated with the $M^2AV$ during the afternoon and the night, which also implies higher energy levels of the PSDs. Canut et al. (2016) also compare 5-hole probe measurements of $M^2AV$ and manned aircraft (Piper Aztec) to sonic anemometer measurements on a tethered-balloon. The TKE measurements from the $M^2AV$ compare well to the tethered balloon measurements (which indirectly compare well to the sonic anemometer on the mast); however, the results show that TKE measured from the manned aircraft were biased towards higher TKEs. Thomas et al. (2012) conclude that direct comparisons between the RPA and the sonic anemometer are tenuous in their study as the Manta RPA flew at 520 m.agl, while the sonic anemometer was only at 10 m.agl. Reineman et al. (2013) is the only study that shows similar vertical wind component PSD between a RPA and a ground-based mast (albeit for a relatively short flight above a flat desert). The main difference between the RPAs listed above and the system described in Reineman et al. (2013) is the INS, as no other group has deployed as precise an INS. Since the energy levels of the PSDs for the configuration presented in this manuscript, are higher, one cannot calculate divergence/convergence; however, the PSDs from the measurements presented here show slopes approaching the expected -5/3 Kolmogorov regime and the RPA observations reproduce trends in TKE over a range of meteorological conditions. There is certainly more work that needs to be done to improve the turbulence measurements – particularly by improving the INS measurements.

### 4.2 Turbulent kinetic energy

In the atmospheric boundary layer, the turbulent kinetic energy (TKE) quantifies the intensity of turbulence, which controls mixing of the atmosphere (Wyngaard and Coté (1971); Lenschow (1974)). TKE is defined as:

$$TKE = \frac{1}{2}({\sigma_u}^2 + {\sigma_v}^2 + {\sigma_w}^2) \tag{6}$$

with ${\sigma_u}^2$ as the variance of E-W wind, ${\sigma_v}^2$ as the variance of N-S wind, and ${\sigma_w}^2$ as the variance of vertical wind. To assess TKE values between the wind-RPA ($TKE_{RPA}$) and the sonic anemometers on the mast ($TKE_{mast}$), we compare different horizontal atmospheric length scales. As the length of each RPA leg is 1600 m, multiples of these legs are chosen for comparison with the sonic anemometers (i.e., 800 m, 1600 m, 3200 m, 4800 m, 6400 m). The averaging time necessary for the sonic anemometers to record an airmass traveling an equivalent length is calculated using the observed horizontal wind speed and temporally centered with respect to the RPA leg. Mast observations at 30 or 60 m.agl are selected based on data availability (Table 2). Figure 9 clearly shows significant differences between mast-based ${\sigma_u}^2$ (E-W wind component) and ${\sigma_v}^2$ (N-S wind component) at different altitudes and length scales. Such differences, particularly at 30 m.agl, are related to surface topography (e.g., terrain, nearby trees and fields). Meanwhile, Fig.9 confirms that ${\sigma_u}^2$ and ${\sigma_v}^2$ are similar at 60 m.agl (i.e., isotropy in the N-S and E-W directions), which can be used to assess the performance of the 5-hole probe/INS on the RPA. Results show that $TKE_{RPA}$ are initially higher than $TKE_{mast}$ (open diamond markers in Fig.10), as $u$ (the transversal wind component) shows higher variances than $v$ (as described in Section 4.1). Applying the observed isotropy shown in Fig.9 ($\sigma^2_{u,RPA} = \sigma^2_{v,RPA}$ at 60 m.agl ) for the RPA observations, the comparison of $TKE_{RPA}$ and $TKE_{mast}$ improves (Fig.10; solid diamond markers) by replacing ${\sigma_u}^2$ by ${\sigma_v}^2$ in the calculation of $TKE_{RPA}$. We note, however, the isotropic conditions are not always satisfied (i.e., longitudinal wind rolls affecting crosswind fluxes reported in Reineman et al. (2016)). Consequently, a RPA flight strategy, such as parallel and cross-wind legs, is essential in identifying isotropic conditions and measurement errors associated with the 5-hole probe/INS system.

As mentioned in Section 4.1, studies that report TKE have been published that compare the SUMO and $M^2AV$ to the sonic anemometer at CRA, Lannemezan (Båserud et al. (2016); Lampert et al. (2016)). The reported values of TKE from both of these studies are within 50 % of TKE from the sonic anemometer. Canut et al. (2016) also show a relatively good agreement of TKE between a tethered balloon, the $M^2AV$, and the manned aircraft with a correlation coefficient $R^2$ = 0.88. In this study, for the comparison between the wind-RPA and sonic anemometers (Fig.10), the slope of the linear regression for the RPA observations is 1.32 ($R^2$ = 0.97) and improves to 0.95 ($R^2$ = 0.91) with the isotropy assumption ($\sigma^2_{u,RPA} = \sigma^2_{v,RPA}$). Flight 4 is not included in this analysis because of known issues related to flight performance. These results suggest that improving the measurement of horizontal winds and reducing biases in the horizontal components of the variances may be achieved by 1) improvement of the INS heading measurement (also noted in Elston et al. (2015)), and 2) verified with a cross-leg flight plan (i.e., orthogonal legs).

### 4.3 Vectical wind velocity distributions

To compare vertical wind from the RPA to the sonic anemometer, angle of attack $\alpha$ and pitch angle $\theta$ are re-centered such that average vertical velocity $w$ is 0 m s$^{-1}$ over the time of the flight. This step is needed because the alignment of the 5-hole probe relative to Earth's frame may change with meteorological conditions (such as wind speed) and flight parameters (such as airspeed and nominal pitch angles). The re-centering step of the 5-hole probe on the RPA is further justified by results from the sonic anemometers on the mast, which also show an average vertical velocity approaching 0 m s$^{-1}$ over the duration of the flight. Distributions of vertical wind velocities from the RPA and sonic anemometer at 60 m.agl are compared, and the intersection method is used to quantify the agreement between the distributions. An example of the vertical wind distributions are shown in Fig. 8 for Flight 5. The calculation of the intersection number is obtained from $\sum_{i=1}^{N} min(I_i, M_i)$ with $I$ and $M$ as the normalized distributions to be compared, and $N$ as the total number of bins. For an exact match, the intersection method result is unity, for a complete mismatch, the result is zero. Table 2 summarizes the intersection numbers between the RPA and sonic anemometer vertical wind distributions for the five flights. The intersection numbers between RPA and anemometer vertical wind distributions are higher than 70 %. As expected, this value is lower during Flight 4.

## 5 Comparison of vertical wind velocities from RPA and cloud radar

A BACCHUS field campaign took place at the Mace Head Atmospheric Research Station on the west coast of Galway, Ireland in August 2015. The purpose was to study aerosol-cloud interactions (ACI) linking ground-based and satellite observations using RPAS (Sanchez et al., 2017). Among the four instrumented RPAs which flew at Mace Head, the wind-RPA was equipped with a 5-hole probe and an INS to obtain vertical wind velocities, as well as upward and downward facing pyranometers to identify cloud sampling periods. During the campaign, we concentrated on measurements of vertical wind velocity near cloud base or within clouds to study ACI. After identifying the cloud base from the ceilometer or based on a vertical profile of an earlier flight, the wind-RPA was sent to an altitude close to cloud base, flying 6 km-long straight-and-level legs. Horizontal wind speeds varied from 6 to 12 m s$^{-1}$ from the West during the case studies presented here. During this field campaign, the wind-RPA flew in 10 of the 45 scientific flights for a total of 15 hours. Of the 10 flights with the wind-RPA, three flights contained a complete set of observations (vertical winds, pyanometers, and cloud radar measurements). The other flights were not selected for a number of reasons: water in the 5-hole probe (2 flights), insufficient number of cloud radar data for comparison (2 flights), no cloud (1 flight), no pyranometer data to identify clouds (1 flight), and aborted mission due to strong winds (> 15 m s$^{-1}$, 1 flight). In this section, we focus on three flights with the wind-RPA (Table 3), in which the vertical wind from the RPA is compared to vertical wind from the cloud radar at Mace Head.

The Doppler cloud radar (Cloud Radar MIRA-35, METEK, 35.5-GHz, Ka band) at the Mace Head Research Station is adapted to the observation of the cloud structure (Görsdorf et al., 2015). The cloud radar is equipped with a vertically pointed

antenna with a polarization filter, a magnetron transmitter and two receivers for discerning polarized signals. Measurements are available up to 15-km height for a temporal resolution of 10 seconds. The vertical resolution of the cloud radar is 29 m. In this study, cloud radar data from the cloud top or the RPA flight altitude are selected for the comparison.

While the flight altitude for the wind-RPA was estimated to be near the cloud base, uncertainties in retrieving cloud base height or an evolution in cloud base height related to diurnal cycles of the boundary layer inevitably lead to the RPA flying in the clouds rather than below cloud base. Note that direct comparison of instantaneous data between the RPA and cloud radar is not possible, as the RPA did not fly directly over the cloud radar and did not observe the same air mass. Moreover, the cloud radar reports vertical velocities every 10 s (and only when a cloud is present); therefore, relatively long averaging periods are needed to compare vertical velocity distributions of the cloud radar with RPA observations. In this section, we present selected time series of the cloud radar measurements that represent the state of the atmosphere during the flight; for cases with sufficient cloud cover, we present different averaging periods of the cloud radar (a short period that coincides with the RPA flight and longer periods for better counting statistics). In the present study, normalized vertical wind velocity distributions of the cloud radar serve to validate the RPA results. In addition, the vertical velocity distributions provide insight on different atmospheric states (e.g., in/out of cloud, over water/land).

### 5.1 Stratocumulus deck with light precipitation (Flight 26: 2015/08/11)

On 11 August, the sky was covered by a lightly precipitating stratocumulus deck, and the wind-RPA flew at 1160 m.asl (about 100 m above the cloud base). The time series of vertical wind from the cloud radar is presented in Fig.11, along colored horizontal lines that indicate observation periods of the cloud radar and RPA. Figure 12 presents a comparison of the normalized vertical wind distributions obtained by cloud radar and the RPA measurements. The standard deviation of RPA vertical wind distribution is $\sigma_{RPA}$ = 0.19 m s$^{-1}$ (or 0.10 m s$^{-1}$ if only positive vertical velocities are considered). This result is comparable to the range of vertical wind standard deviations obtained in Lu et al. (2007) for stratocumulus clouds observed off the coast of Monterey, California, in the Eastern Pacific ($0.06 < \sigma_w < 0.29$ m s$^{-1}$, for $w > 0$ m s$^{-1}$ from 11 sampled stratocumulus clouds). In this case study, the presence of falling cloud droplets to an altitude as low as 300 m.agl (Fig.11) negatively biases the vertical wind distribution retrieved from the cloud radar (Fig.12). Previous measurements have also shown that precipitation negatively biases cloud radar observations of vertical wind velocities, as the radar indirectly measures vertical wind by using the motion of scatterers (i.e., hydrometeors; Lothon et al. (2005), Bühl et al. (2015)). These negative biases in retrieved vertical winds are largely removed by obtaining vertical velocity distributions at the top of the cloud (Bühl et al., 2015). Similar results are obtained for our case study, as the cloud radar is strongly influenced by falling droplets, yet only slightly negatively biased at the cloud top. The intersection method, described in Section 4.3, is used to compared the normalized cloud radar vertical wind distributions to those of the RPA (Table 3). The intersection number is 0.53 between cloud radar and observations at the RPA flight altitude. This relatively low match is a result of the negative bias from the precipitating droplets. A much better agreement is found between the cloud radar vertical velocity distribution

retrieved at the cloud top (1360 m.asl) and the RPA measurements (intersection number = 0.74).

### 5.2 Cloud fields with changing meteorology (Flight 38: 2015/08/21)

In this case study, the results from the RPA and cloud radar emphasizes the differences in vertical wind distributions depending on the meteorological conditions related to cloud field. The wind-RPA flew within a cloud above the ocean and in clear sky above land for three legs, after which the local meteorology changed into a formation of developing clouds above land (where a cloudless sky had previously been observed; Fig.13). The vertical wind velocity distributions are presented using a combination of information shown in a series of figures: downwelling and upwelling pyranometer observations, and three periods corresponding to distinct meteorological conditions (Fig.13); the time series of cloud radar data (Fig.14); and the vertical wind distributions from the RPA and the cloud radar (Fig.15). These meteorological periods are defined in Fig.13 as "cloud" (both pyranometers approach similar values), "no cloud" (downwelling pyranometer is significantly higher than upwelling pyranometer), and a third period associated to a developing field of broken clouds (spatially variable downwelling pyranometer). Based on the pyranometer measurements, we deduce a cloudless sky (cyan) was observed by the RPA above land for the first three legs (Fig.13). The cloud radar also did not detect clouds above land for the beginning of the flight (Fig.14). In the meantime, the RPA flew within a cloud above the ocean (Fig.13, green), which was not observed by the cloud radar. Figure 15 shows that the standard deviation of vertical velocity within the cloud is larger than for clear sky conditions ($\sigma_{cloud}$ = 0.28 m s$^{-1}$, $\sigma_{no\,cloud}$ = 0.17 m s$^{-1}$) , which highlights the presence of stronger vertical winds in the presence of clouds. During the last two legs of Flight 38, the wind-RPA flew through a developing field of broken clouds above land (Fig.13, magenta), which also appeared in the cloud radar time series and in the satellite image (Fig.4 in Sanchez et al. (2017)). The standard deviation during the "broken cloud" RPA period is larger than the other periods ($\sigma_{broken\,cloud}$ = 0.46 m s$^{-1}$), and the shape of vertical wind distributions is similar for both the cloud radar and the RPA (Fig.15). While not shown here, the vertical wind distributions observed by the cloud radar are similar at cloud base (380 m.asl) and at the flight altitude (660 m.asl), as well as over different lengths of observing periods (1.5 and 4 hours). In Table 3, intersection numbers illustrate the relatively close matches (ca. 80 %) in comparing the "broken cloud" RPA period and the cloud radar for 4 hours (radar flight altitude) and for 1.5 hours (radar flight time). The similar results for the observations of a field of broken clouds independently reinforces RPA and cloud radar observational methods, and the changes in meteorological conditions highlight the ability to identify distinct states of the atmosphere with the RPA.

### 5.3 Fair weather cumulus clouds (Flight 30: 2015/08/15)

During Flight 30, the cloud field was scattered with small clouds as shown in Fig.17 by the cloud radar time series. However, the number of data points from the cloud radar during the flight time (black segment) was insufficient to establish a vertical wind distribution, therefore only the cloud radar data for 4 hours (red segment) are presented in Fig.18. The wind-RPA flew through one of these clouds as shown by the pyranometer measurements in Fig.16. To compare cloud radar and RPA data,

vertical winds from the RPA are again divided into "cloud" and "no-cloud" periods based on pyranometer observations. The respective standard deviations for the periods are $\sigma_{cloud}$ = 0.35 m s$^{-1}$ and $\sigma_{no\,cloud}$ = 0.34 m s$^{-1}$, which are not statistically different. However, the variability between legs is significantly greater in the "no cloud" period (as represented by the envelope in blue dashed lines in Fig.18) compared to the "cloud" period (envelope in green dashed lines). In Fig.18, the RPA and cloud radar measurements show similar results during the "cloud" period, with an intersection number equal to 0.76. Kunz and de Leeuw (2000) have observed an upward component in the air flow at the surface from the ocean at the Mace Head Research Station as a result of the terrain. However, systematic differences between the RPA and cloud radar have not been observed for the other case studies, so we cannot quantify the role of surface heating or orography on the cloud radar vertical distributions compared to those of the RPA.

## 6 Sensitivity of vertical winds on aerosol-cloud interactions

To study aerosol-cloud interactions, the input parameters for an aerosol-cloud parcel model (ACPM) are obtained from vertical profiles (temperature, relative humidity), straight-and-level legs (updraft), and measurements of cloud condensation nuclei spectra and aerosol size distributions. A weighted ensemble of updraft velocities, based on 5-hole probe measurements, is used in the parcel model to simulate the cloud droplet distribution, (Sanchez et al. (2016); Sanchez et al. (2017)). A sensitivity study assesses the impact of the vertical velocity distributions between the RPA and anemometer (Section 4)/cloud radar (Section 5) on the resulting cloud droplet number concentrations for populations. The sensitivity is equal to $1/N.dN/dw$ with $N$ the cloud droplet number concentration and $dN/dw$ the slope of the cloud droplet number/updraft relationships found in Martin et al. (2017); Ming et al. (2006). The resulting cloud droplet number concentration is more sensitive at low concentrations ($\sim 1/N$) and at low updraft velocities (when $dN/dw$ is the largest). Based on polluted and clean cases described in Martin et al. (2017), cloud droplet numbers are ca. 100 and 350 cm$^{-3}$, respectively, with relative differences owing to RPA and anemometer/cloud radar updraft velocities within 10 %. While the cloud droplet number concentration simulated with the RPA measurements is systematically higher than from sonic anemometer owing to the broader RPA vertical velocity distributions, a systematic difference in cloud droplet number concentrations is not observed between the RPA and cloud radar. These results suggest that the updraft measurements based on RPA measurements are sufficiently accurate for representing aerosol-cloud interactions.

## 7 Conclusions

The validation of vertical wind measurements in clouds measured by a 5-hole probe on a lightweight remotely piloted aircraft (RPA) has been detailed in this study. Atmospheric winds in the Earth's coordinate system are derived using the equations described in Lenschow and Spyers-Duran (1989) with an inertial navigation system (INS) to remove RPA motion from the wind vectors measured by the 5-hole probe. The 5-hole probe has been calibrated in wind tunnel on a two-axis platform to

obtain the angle of attack, angle of sideslip and airspeed of the RPA. Motions induced by the dynamic platform in the wind-tunnel were effectively removed, thereby validating probe/INS performance. Nonetheless, the rate of the angular rotation of the platform does impact the precision of derived atmospheric winds. The uncertainty associated with the vertical wind measurement $w$ is determined to be 0.12 m $s^{-1}$ using a Gaussian error propagation analysis (and uncertainty related to horizontal wind is 1.1 m $s^{-1}$ based on reverse-heading maneuvers). Vertical velocity distributions from the RPA and sonic anemometers show intersection values higher than 70 % in calm wind conditions. Comparisons have also been made between power spectral density (PSD) functions of the sonic anemometer and RPA measurements, and demonstrate the impact of optimizing INS heading measurements on the PSD (particularly for the transversal component of wind). The observed isotropy by the sonic anemometer at 60 m.agl is used to improve estimates of turbulent kinetic energy (TKE) obtained from RPA wind measurements. However, orthogonal flight plans must be implemented in order to account for parallel- and cross-wind atmospheric conditions and measurement biases (particularly related to transversal wind components).

Three case studies from a BACCHUS field campaign (at the Mace Head Atmospheric Research Station, Galway, Ireland) validated RPA vertical wind velocities in clouds compared to cloud radar observations. Vertical wind velocity distributions were classified according to the flight periods (e.g., clear sky or cloud), emphasizing the impact of meteorology and the state of the atmosphere on the distribution of vertical wind velocities in the cloud field. For the first case study, a stratocumulus deck covered the sky and light precipitation was observed. Cloud radar vertical wind velocity distribution was negatively biased and cloud base was not distinctly visible due to falling droplets. The wind-RPA provided a centered vertical wind distribution near cloud base, which was similar to cloud radar observations at cloud-top (in the non-precipitating region of the cloud). The second case study displayed different meteorological conditions during the flight, which were well distinguished by the wind-RPA, including differences between a developing field of broken clouds, a small convective cloud, and clear sky. In the third case study, similar vertical wind distributions in clouds were observed by the RPA and the cloud radar in fair weather cumulus cloud systems above land and ocean. The vertical velocity distributions, which were encountered for each of the case studies, highlighted the ability of the RPA platform to differentiate the meteorological conditions associated with the cloud systems based on vertical wind measurements.

To estimate the impact of discrepancies in vertical wind distributions on cloud droplet number concentrations, a sensitivity study was conducted to assess the relationship between cloud droplet number concentrations and updraft for different aerosol populations. The difference in vertical wind distributions between RPA and anemometer/cloud radar generally resulted in differences less than 10 %. These results demonstrate that vertical velocity measurements on the RPA are sufficiently accurate to conduct aerosol-cloud closure studies using RPAs.

*Acknowledgements.* The research leading to these results received funding from the European Union's Seventh Framework Programme (FP7/2007-2013) project BACCHUS under grant agreement n°603445. NUI Galway was also supported by the HEA under PRTLI4, the

EPA, and SFI through the MaREI Centre. Part of the remotely piloted aircraft system operations presented here have been conducted at Centre de Recherches Atmosphériques of Lannemezan (an instrumented site of the Pyrenean Platform of Observation of the Atmosphere, P2OA), supported by the University Paul Sabatier, Toulouse (France) and CNRS INSU (Institut National des Sciences de l'Univers). The RPAS used for the experiments presented in this work have been developed by the Ecole Nationale de l'Aviation Civile (ENAC). We also thank Marie Lothon from CRA, Lannemezan, Bruno Piguet, William Maurel and Guylaine Canut from Centre National de Recherches Météorologiques (CNRM) for their advices on wind measurements, and Joachim Reuder and Line Båserud from the Geophysical Institute, Univeristy of Bergen, Norway, for their advices on TKE calculation.

## References


Axford, D. N.: On the Accuracy of Wind Measurements Using an Inertial Platform in an Aircraft, and an Example of a Measurement of the Vertical Mesostructure of the Atmosphere, Journal of Applied Meteorology, 7, 645–666, doi:10.1175/1520-0450(1968)007<0645:OTAOWM>2.0.CO;2, 1968.

BACCHUS: BACCHUS, Impact of Biogenic versus Anthropogenic emissions on Clouds and Climate: towards a Holistic UnderStanding, http://www.bacchus-env.eu/, 2016.

Båserud, L., Reuder, J., Jonassen, M. O., Kral, S. T., Paskyabi, M. B., and Lothon, M.: Proof of concept for turbulence measurements with the RPAS SUMO during the BLLAST campaign, Atmospheric Measurement Techniques, 9, 4901–4913, doi:10.5194/amt-9-4901-2016, 2016.

Boiffier, J.: The dynamics of flight, the equations, John Wiley and Sons, iSBN 0 471 94237 5, 1998.

Brisset, P., Drouin, A., Gorraz, M., Huard, P.-S., and Tyler, J.: The Paparazzi Solution, p. pp xxxx, https://hal-enac.archives-ouvertes.fr/hal-01004157, 2006.

Brown, E. N., Friehe, C. A., and Lenschow, D. H.: The Use of Pressure Fluctuations on the Nose of an Aircraft for Measuring Air Motion, Journal of Climate and Applied Meteorology, 22, 171–180, doi:10.1175/1520-0450(1983)022<0171:TUOPFO>2.0.CO;2, 1983.

Bühl, J., Leinweber, R., Görsdorf, U., Radenz, M., Ansmann, A., and Lehmann, V.: Combined vertical-velocity observations with Doppler lidar, cloud radar and wind profiler, Atmospheric Measurement Techniques, 8, 3527–3536, doi:10.5194/amt-8-3527-2015, 2015.

Canut, G., Couvreux, F., Lothon, M., Legain, D., Piguet, B., Lampert, A., Maurel, W., and Moulin, E.: Turbulence fluxes and variances measured with a sonic anemometer mounted on a tethered balloon, Atmospheric Measurement Techniques, 9, 4375–4386, doi:10.5194/amt-9-4375-2016, 2016.

Conant, W. C., VanReken, T. M., Rissman, T. A., Varutbangkul, V., Jonsson, H. H., Nenes, A., Jimenez, J. L., Delia, A. E., Bahreini, R., Roberts, G. C., Flagan, R. C., and Seinfeld, J. H.: Aerosol–cloud drop concentration closure in warm cumulus, Journal of Geophysical Research: Atmospheres, 109, n/a–n/a, doi:10.1029/2003JD004324, d13204, 2004.

Elston, J., Argrow, B., Stachura, M., Weibel, D., Lawrence, D., and Pope, D.: Overview of Small Fixed-Wing Unmanned Aircraft for Meteorological Sampling, Journal of Atmospheric and Oceanic Technology, 32, 97–115, doi:10.1175/JTECH-D-13-00236.1, 2015.

Garman, K. E., Hill, K. A., Wyss, P., Carlsen, M., Zimmerman, J. R., Stirm, B. H., Carney, T. Q., Santini, R., and Shepson, P. B.: An Airborne and Wind Tunnel Evaluation of a Wind Turbulence Measurement System for Aircraft-Based Flux Measurements, Journal of Atmospheric and Oceanic Technology, 23, 1696–1708, doi:10.1175/JTECH1940.1, 2006.

Görsdorf, U., Lehmann, V., Bauer-Pfundstein, M., Peters, G., Vavriv, D., Vinogradov, V., and Volkov, V.: A 35-GHz Polarimetric Doppler Radar for Long-Term Observations of Cloud Parameters—Description of System and Data Processing, Journal of Atmospheric and Oceanic Technology, 32, 675–690, doi:10.1175/JTECH-D-14-00066.1, 2015.

Khelif, D., Burns, S. P., and Friehe, C. A.: Improved Wind Measurements on Research Aircraft, Journal of Atmospheric and Oceanic Technology, 16, 860–875, doi:10.1175/1520-0426(1999)016<0860:IWMORA>2.0.CO;2, 1999.

Kunz, G. and de Leeuw, G.: Micrometeorological characterisation of the Mace Head field station during PARFORCE, in New Particle Formation and Fate in the Coastal Environment, Rep. Ser. in Aerosol Sci., edited by C. D. O'Dowd and K. Hämeri, vol.48, 2000.

Lampert, A., Pätzold, F., Jiménez, M. A., Lobitz, L., Martin, S., Lohmann, G., Canut, G., Legain, D., Bange, J., Martínez-Villagrasa, D., and Cuxart, J.: A study of local turbulence and anisotropy during the afternoon and evening transition with an unmanned aerial system and mesoscale simulation, Atmospheric Chemistry and Physics, 16, 8009–8021, doi:10.5194/acp-16-8009-2016, 2016.

Lenschow, D. and Spyers-Duran, P.: Measurement Techniques : Air motion sensing, National Center for Atmospheric Research, Bulletin No.23, https://www.eol.ucar.edu/raf/Bulletins/bulletin23.html, 1989.

Lenschow, D. H.: Model of the Height Variation of the Turbulence Kinetic Energy Budget in the Unstable Planetary Boundary Layer, Journal of the Atmospheric Sciences, 31, 465–474, doi:10.1175/1520-0469(1974)031<0465:MOTHVO>2.0.CO;2, 1974.

Lothon, M., Lenschow, D. H., Leon, D., and Vali, G.: Turbulence measurements in marine stratocumulus with airborne Doppler radar, Quarterly Journal of the Royal Meteorological Society, 131, 2063–2080, doi:10.1256/qj.04.131, 2005.

Lothon, M., Lohou, F., Pino, D., Couvreux, F., Pardyjak, E. R., Reuder, J., Vilà-Guerau de Arellano, J., Durand, P., Hartogensis, O., Legain, D., Augustin, P., Gioli, B., Lenschow, D. H., Faloona, I., Yagüe, C., Alexander, D. C., Angevine, W. M., Bargain, E., Barrié, J., Bazile, E., Bezombes, Y., Blay-Carreras, E., van de Boer, A., Boichard, J. L., Bourdon, A., Butet, A., Campistron, B., de Coster, O., Cuxart, J., Dabas, A., Darbieu, C., Deboudt, K., Delbarre, H., Derrien, S., Flament, P., Fourmentin, M., Garai, A., Gibert, F., Graf, A., Groebner, J., Guichard, F., Jiménez, M. A., Jonassen, M., van den Kroonenberg, A., Magliulo, V., Martin, S., Martinez, D., Mastrorillo, L., Moene, A. F., Molinos, F., Moulin, E., Pietersen, H. P., Piguet, B., Pique, E., Román-Cascón, C., Rufin-Soler, C., Saïd, F., Sastre-Marugán, M., Seity, Y., Steeneveld, G. J., Toscano, P., Traullé, O., Tzanos, D., Wacker, S., Wildmann, N., and Zaldei, A.: The BLLAST field experiment: Boundary-Layer Late Afternoon and Sunset Turbulence, Atmospheric Chemistry and Physics, 14, 10 931–10 960, doi:10.5194/acp-14-10931-2014, 2014.

Lu, M.-L., Conant, W. C., Jonsson, H. H., Varutbangkul, V., Flagan, R. C., and Seinfeld, J. H.: The Marine Stratus/Stratocumulus Experiment (MASE): Aerosol-cloud relationships in marine stratocumulus, Journal of Geophysical Research: Atmospheres, 112, n/a–n/a, doi:10.1029/2006JD007985, d10209, 2007.

Martin, A. C., Cornwell, G. C., Atwood, S. A., Moore, K. A., Rothfuss, N. E., Taylor, H., DeMott, P. J., Kreidenweis, S. M., Petters, M. D., and Prather, K. A.: Transport of pollution to a remote coastal site during gap flow from California's interior: impacts on aerosol composition, clouds, and radiative balance, Atmospheric Chemistry and Physics, 17, 1491–1509, doi:10.5194/acp-17-1491-2017, 2017.

Ming, Y., Ramaswamy, V., Donner, L. J., and Phillips, V. T. J.: A New Parameterization of Cloud Droplet Activation Applicable to General Circulation Models, Journal of the Atmospheric Sciences, 63, 1348–1356, doi:10.1175/JAS3686.1, 2006.

Peng, Y., Lohmann, U., and Leaitch, R.: Importance of vertical velocity variations in the cloud droplet nucleation process of marine stratus clouds, Journal of Geophysical Research: Atmospheres, 110, n/a–n/a, doi:10.1029/2004JD004922, d21213, 2005.

Reineman, B. D., Lenain, L., Statom, N. M., and Melville, W. K.: Development and Testing of Instrumentation for UAV-Based Flux Measurements within Terrestrial and Marine Atmospheric Boundary Layers, Journal of Atmospheric and Oceanic Technology, 30, 1295–1319, doi:10.1175/JTECH-D-12-00176.1, 2013.

Reineman, B. D., Lenain, L., and Melville, W. K.: The Use of Ship-Launched Fixed-Wing UAVs for Measuring the Marine Atmospheric Boundary Layer and Ocean Surface Processes, Journal of Atmospheric and Oceanic Technology, 33, 2029–2052, doi:10.1175/JTECH-D-15-0019.1, https://doi.org/10.1175/JTECH-D-15-0019.1, 2016.

Reuder, J., Ablinger, M., Ágústsson, H., Brisset, P., Brynjólfsson, S., Garhammer, M., Jóhannesson, T., Jonassen, M. O., Kühnel, R., Lämmlein, S., de Lange, T., Lindenberg, C., Malardel, S., Mayer, S., Müller, M., Ólafsson, H., Rögnvaldsson, Ó., Schäper, W., Spengler, T., Zängl, G., and Egger, J.: FLOHOF 2007: an overview of the mesoscale meteorological field campaign at Hofsjökull, Central Iceland, Meteorology and Atmospheric Physics, 116, 1–13, doi:10.1007/s00703-010-0118-, 2012.

Reuder, J., Båserud, L., Jonassen, M. O., Kral, S. T., and Müller, M.: Exploring the potential of the RPA system SUMO for multipurpose boundary-layer missions during the BLLAST campaign, Atmospheric Measurement Techniques, 9, 2675–2688, doi:10.5194/amt-9-2675-2016, 2016.

Sanchez, K., Roberts, G., Calmer, R., Nicoll, K., Harshimshoni, E., Rosenfeld, D., Ovadnevaite, J., Preissler, J., Ceburnis, D., O'Dowd, C., and Russell, L.: Top-down and bottom-up aerosol-cloud-closure: towards understanding sources of uncertainty in deriving cloud radiative forcing, Atmos. Chem. Phy., doi:10.5194/acp-2017-201, 2017, 2017.

Sanchez, K. J., Russell, L. M., Modini, R. L., Frossard, A. A., Ahlm, L., Corrigan, C. E., Roberts, G. C., Hawkins, L. N., Schroder, J. C., Bertram, A. K., Zhao, R., Lee, A. K. Y., Lin, J. J., Nenes, A., Wang, Z., Wonaschütz, A., Sorooshian, A., Noone, K. J., Jonsson, H., Toom, D., Macdonald, A. M., Leaitch, W. R., and Seinfeld, J. H.: Meteorological and aerosol effects on marine cloud microphysical properties, Journal of Geophysical Research: Atmospheres, 121, 4142–4161, doi:10.1002/2015JD024595, 2016.

Spiess, T., Bange, J., Buschmann, M., and Vörsmann, P.: First application of the meteorological Mini-UAV 'M2AV', Meteorologische Zeitschrift, 16, 159–169, doi:10.1127/0941-2948/2007/0195, 2007.

Sullivan, S. C., Lee, D., Oreopoulos, L., and Nenes, A.: Role of updraft velocity in temporal variability of global cloud hydrometeor number, Proceedings of the National Academy of Sciences, 113, 5791–5796, doi:10.1073/pnas.1514039113, 2016.

Thomas, R. M., Lehmann, K., Nguyen, H., Jackson, D. L., Wolfe, D., and Ramanathan, V.: Measurement of turbulent water vapor fluxes using a lightweight unmanned aerial vehicle system, Atmospheric Measurement Techniques, 5, 243–257, doi:10.5194/amt-5-243-2012, 2012.

Treaster, A. L. and Yocum, A. M.: The calibration and application of five-hole probes, NASA STI/Recon Technical Report N, 78, 1978.

van den Kroonenberg, A., Martin, T., Buschmann, M., Bange, J., and Vörsmann, P.: Measuring the Wind Vector Using the Autonomous Mini Aerial Vehicle M2AV, Journal of Atmospheric and Oceanic Technology, 25, 1969–1982, doi:10.1175/2008JTECHA1114.1, 2008.

Wildmann, N., Ravi, S., and Bange, J.: Towards higher accuracy and better frequency response with standard multi-hole probes in turbulence measurement with remotely piloted aircraft (RPA), Atmospheric Measurement Techniques, 7, 1027–1041, doi:10.5194/amt-7-1027-2014, 2014.

Wyngaard, J. C. and Coté, O. R.: The Budgets of Turbulent Kinetic Energy and Temperature Variance in the Atmospheric Surface Layer, Journal of the Atmospheric Sciences, 28, 190–201, doi:10.1175/1520-0469(1971)028<0190:TBOTKE>2.0.CO;2, 1971.

**Table 1.** Uncertainty (1-$\sigma$) associated with parameters from 5-hole probe (5HP) and inertial navigation system (INS) for the calculation of error associated with the vertical wind velocity $w$.

| Variable | Symbol | precision/value |
|---|---|---|
| differential pressure between holes 1 and 6 (5HP) | $\sigma_{\Delta(P_1-P_6)}$ | 0.012 mbar |
| differential pressure between holes 2 and 3 (5HP) | $\sigma_{\Delta(P_2-P_3)}$ | 0.014 mbar |
| differential pressure between holes 4 and 5 (5HP) | $\sigma_{\Delta(P_4-P_5)}$ | 0.012 mbar |
| ratio of differential pressures (5HP) | $\sigma_{C_\alpha}$ | 0.013 |
| angle of attack (5HP) | $\sigma_\alpha$ | 0.16 deg |
| pitch angle (INS) | $\sigma_\theta$ | 0.25 deg |
| airspeed (5HP) | $\sigma_{V_a}$ | 0.1 m s$^{-1}$ systematic 7 % |
| vertical RPA speed (INS) | $\sigma_{V_z}$ | 0.1 m s$^{-1}$ |
| coefficient calibration - slope | $a_\alpha$ | 12.52 |
| coefficient calibration - intersect | $b_\alpha$ | 0.039 |
| uncertainty related to vertical wind velocity | $\sigma_w$ | 0.12 m s$^{-1}$ |

**Table 2.** Description of flights conducted at CRA, Lannemezan, France.

| ID | Date | Time (local) | Duration | Horizontal wind speed | Wind direction | Intersection number* | Remarks |
|---|---|---|---|---|---|---|---|
| Flight 1 | 15 Oct 2015 | 08:05 | 1h30 | 0.6 m s$^{-1}$ | NE | 0.72 | sonic anemometer at 30 m.agl only |
| Flight 2 | 15 Oct 2015 | 12:47 | 1h22 | 1.9 m s$^{-1}$ | N | 0.79 | sonic anemometer at 30 m.agl only |
| Flight 3 | 15 Oct 2015 | 15:35 | 1h18 | 2.7 m s$^{-1}$ | NW | 0.90 | sonic anemometer at 30 m.agl only |
| Flight 4 | 20 May 2016 | 09:15 | 1h35 | 3.2 m s$^{-1}$ | SW | 0.71 | airspeed close to stall speed |
| Flight 5 | 7 Jul 2016 | 15:18 | 1h06 | 1.7 m s$^{-1}$ | NE | 0.88 | optimized INS |

*intersection number described in Section 4.3

**Table 3.** Description of BACCHUS case study flights, Mace Head Research Station, Ireland. The intersection number compares vertical wind velocity distributions between RPA and cloud radar.

| | | | | | | Intersection number** (comparison with RPA) | | | |
|---|---|---|---|---|---|---|---|---|---|
| ID | Date | Time (local) | Duration | Horizontal wind speed | wind direction | radar flight alt. | radar flight time | radar cloud top | Figure |
| Flight 26* | 11 Aug 2015 | 16:17 | 1h20 | 6 m $s^{-1}$ | WNW to SW | 0.53 | 0.67 | 0.74 | Fig.12 |
| Flight 30 | 15 Aug 2015 | 14:19 | 50 min | 10 m $s^{-1}$ | W to WSW | 0.77 | — | — | Fig.18 |
| Flight 38 | 21 Aug 2015 | 16:10 | 1h30 | 10 m $s^{-1}$ | SSW | 0.81 | 0.76 | — | Fig.15 |

*no pyranometer data

**intersection number described in Section 4.3

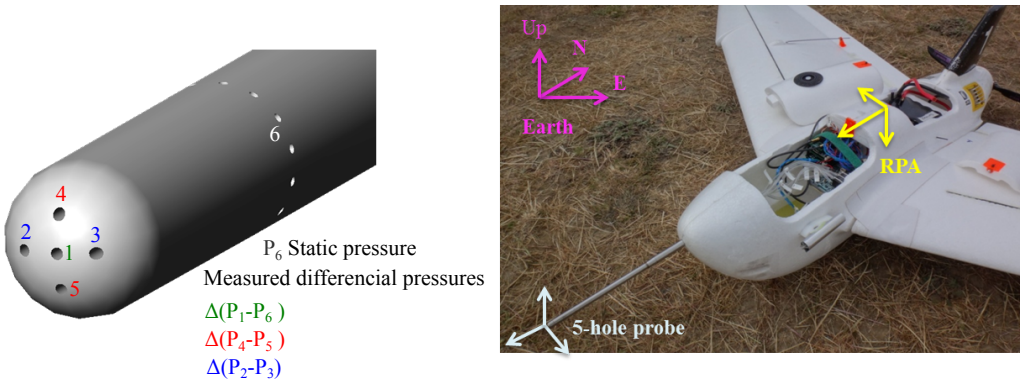


(a) (b)

**Figure 1.** (a) 5-hole probe tip, schematic representation of pressure holes. (b) 5-hole probe mounted on a Skywalker X6 RPA.

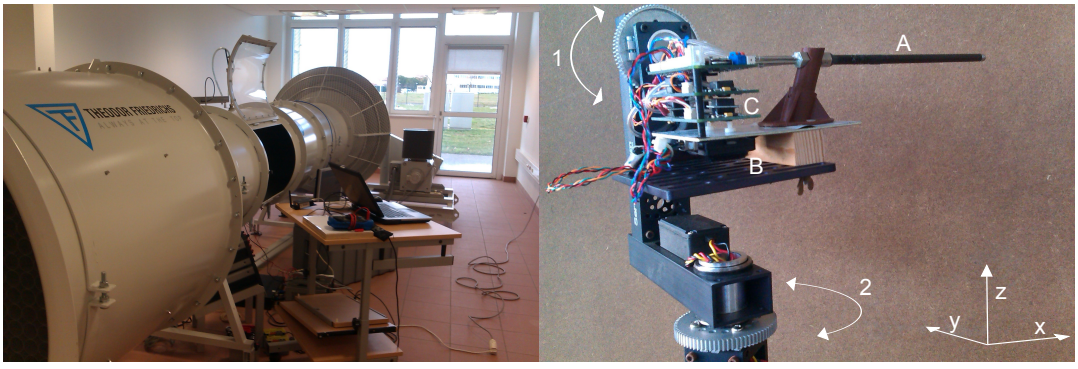


(a) (b)

**Figure 2.** (a) Theodor Friedrichs wind tunnel, Météo-France, Toulouse. (b) Two-axis platform for wind tunnel experiment, 1: rotation on pitch axis, 2: rotation on yaw axis, A: 5-hole probe, B: INS, C: pressure sensors.

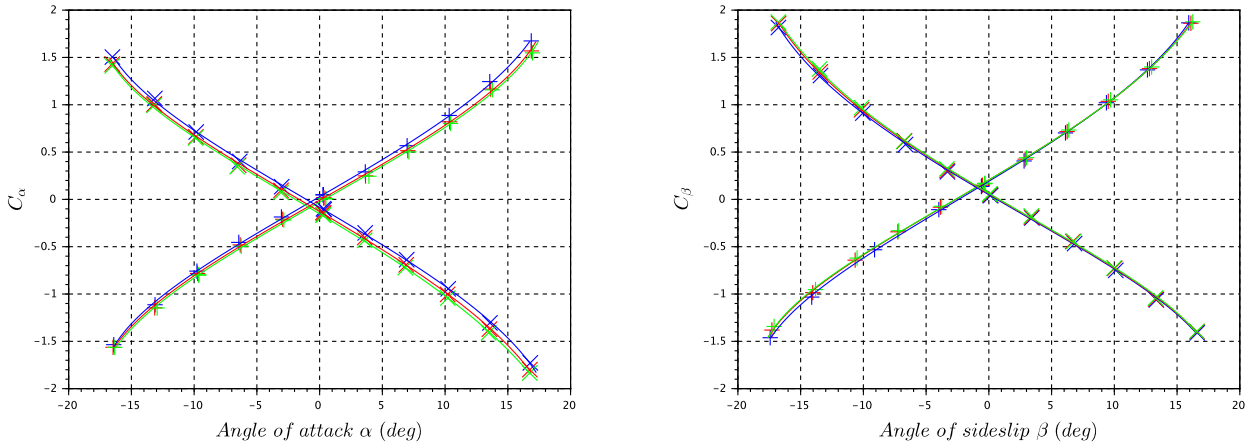


(a) (b)

**Figure 3.** (a) Calibration coefficients $C_\alpha$ for the calculation of the angle of attack $\alpha$ (INS pitch angles as a reference) at different wind tunnel velocities, blue: 15 m s$^{-1}$, red: 20 m s$^{-1}$, green: 25 m s$^{-1}$. The positive slope corresponds to the probe in standard orientation, + markers. The negative slope corresponds to the probe in inverted orientation, x markers. (b) Calibration coefficients $C_\beta$ for the calculation of the angle of sidesplit $\beta$ (INS yaw angles as a reference) at different wind tunnel velocities, blue: 15 m s$^{-1}$, red: 20 m s$^{-1}$, green: 25 m s$^{-1}$. The positive slope corresponds to the probe in standard orientation, + markers. The negative slope corresponds to the probe in inverted orientation, x markers.

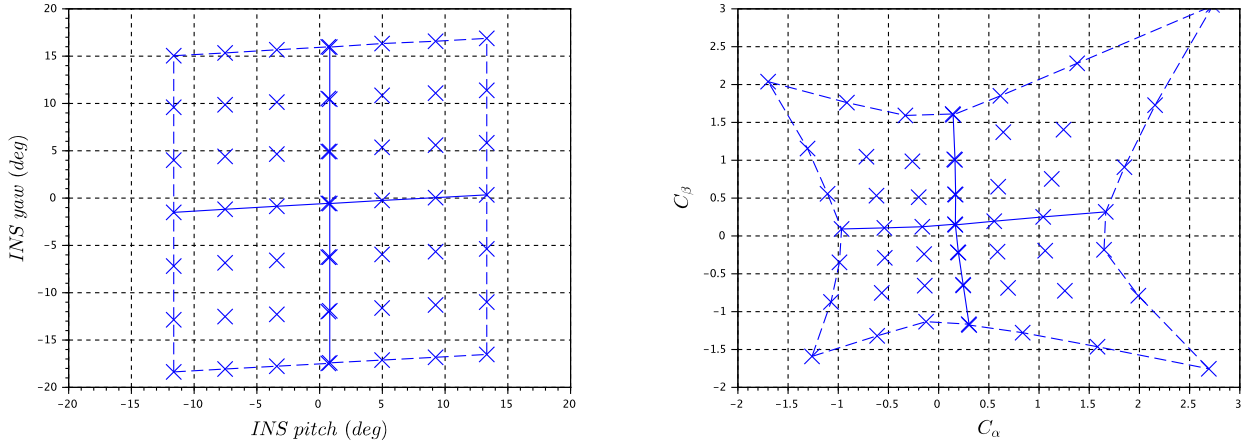


(a) (b)

**Figure 4.** (a) Variation by step of pitch and yaw angles of the two-axis platform in wind tunnel, airspeed 15 m s$^{-1}$. (b) Corresponding $C_\alpha$ and $C_\beta$ of the 5-hole probe to steps of the platform.

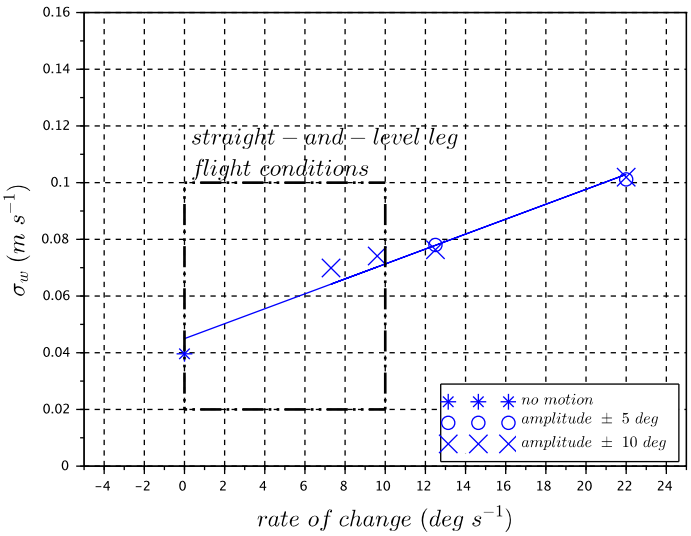


**Figure 5.** Standard deviation of vertical wind vector $w$ for each rate of change of the pitch angles on the two-axis platform. For the flight along straight-and-level legs, the rate of change does not exceed 10 deg $s^{-1}$.

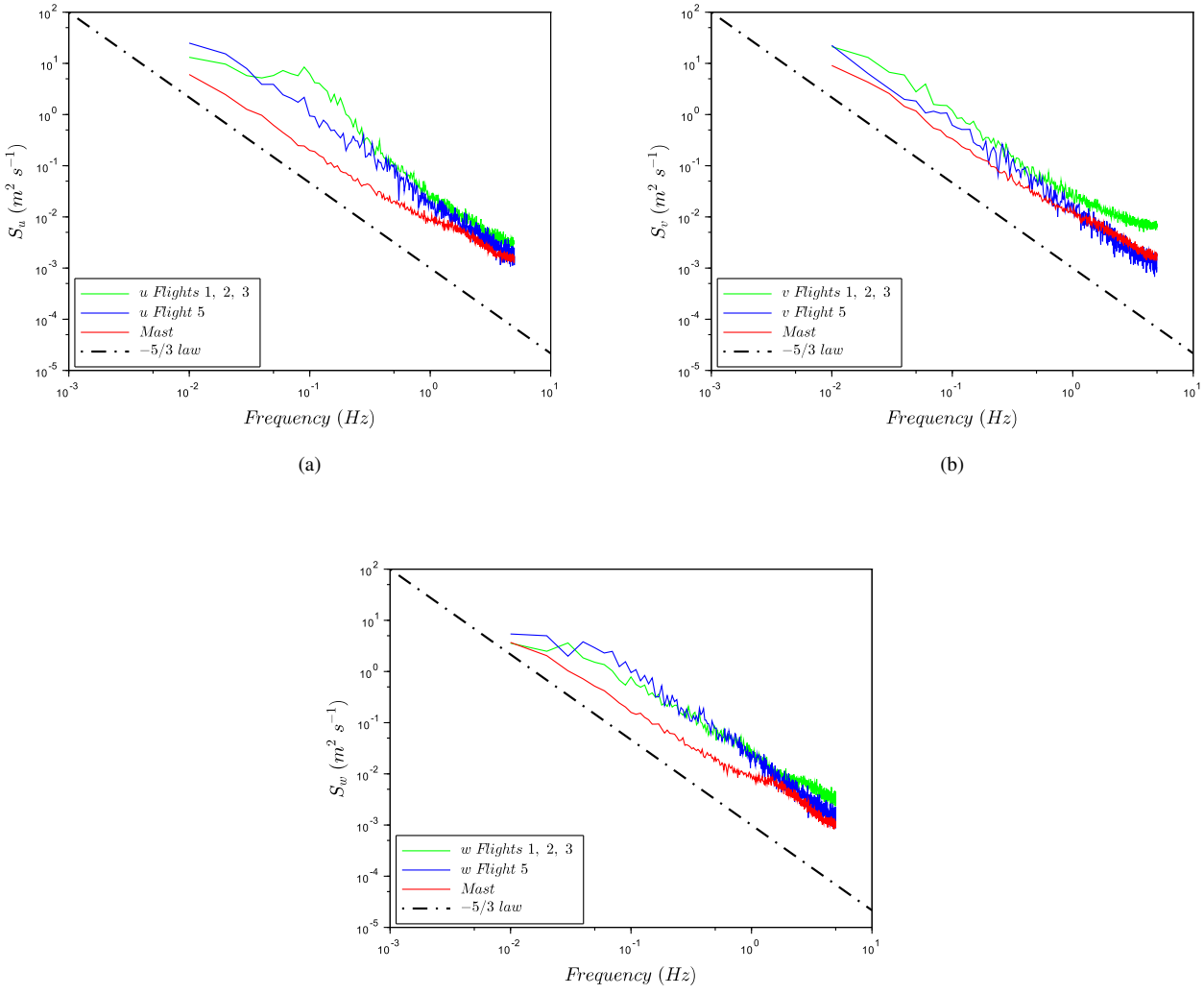


**Figure 6.** Comparison of averaged PSDs from sonic anemometers (Mast : red) and RPA wind measurements averaged for Flights 1, 2 and 3 (green), and Flight 5 (blue) after the INS has been optimized. The dashed line represents the $f^{-5/3}$ law. (a) Spectral energy $S$ of $u$-wind component function of frequency, (b) Spectral energy $S$ of $v$-wind component function of frequency, (c) Spectral energy $S$ of $w$-wind component function of frequency.

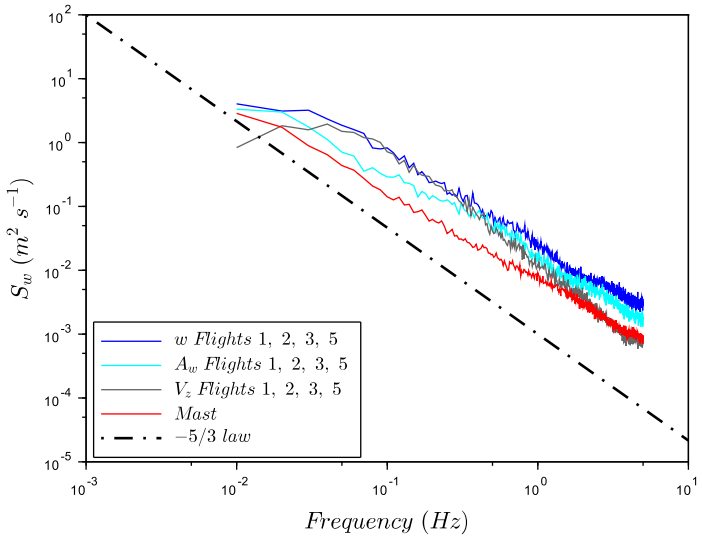


**Figure 7.** Comparison of averaged PSDs from sonic anemometers (Mast : red) and RPA wind measurements averaged for Flights 1, 2, 3 and 5 (blue). Spectral energy $S$ of decomposed $w$-wind component with $w = A_w$ (cyan) + $V_z$ (grey) function of frequency. The dashed line represents the $f^{-5/3}$ law.

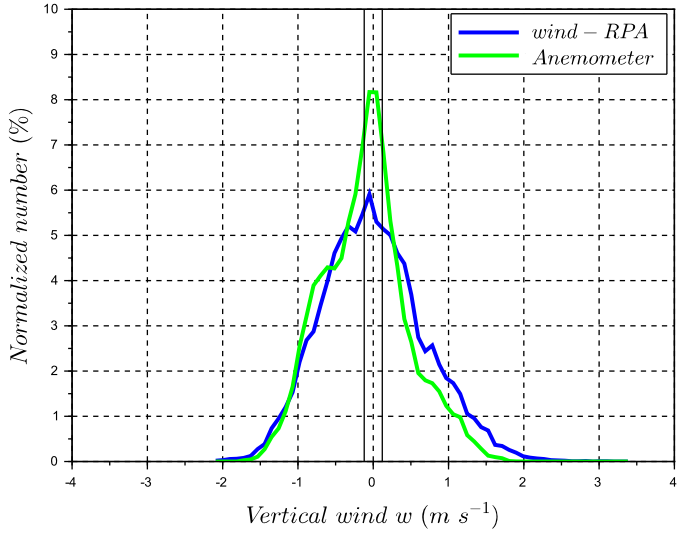


**Figure 8.** Distribution functions of vertical wind $w$ for RPA and sonic anemometer at 60 m.agl measurements, Flight 5. The vertical bars represent the uncertainty ($\sigma_w$ = 0.12 m s$^{-1}$) associated with RPA vertical wind measurements.

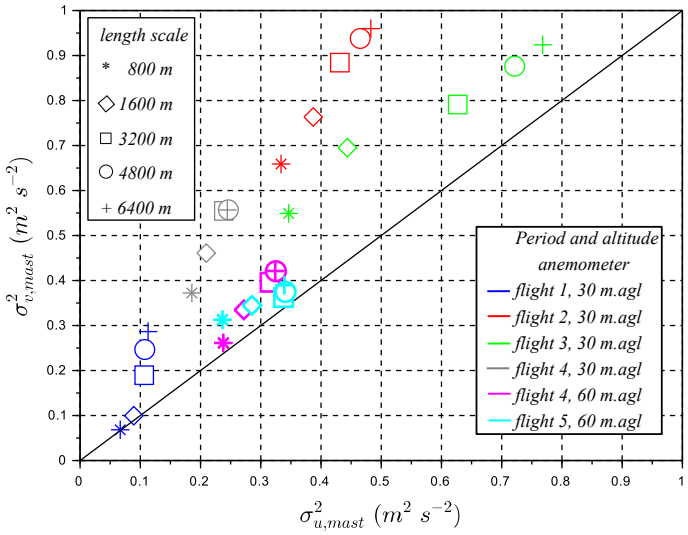


**Figure 9.** Comparison of variances $\sigma^2_{u,mast}$ and $\sigma^2_{v,mast}$ from the sonic anemometers for the associated flight periods and length scales.

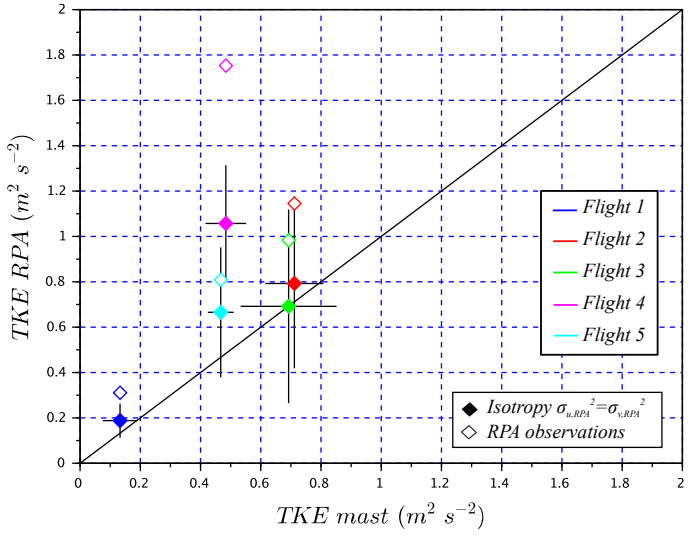


**Figure 10.** Comparison of $TKE_{RPA}$ and $TKE_{mast}$. Open diamonds $TKE_{RPA}$ are calculated with the three wind variances of RPA, solid diamonds are obtained with an isotropy assumption $\sigma^2_{u,RPA} = \sigma^2_{v,RPA}$ observed at 60 m.agl by the sonic anemometer in Fig.9. The uncertainty bars correspond to 1-sigma, using all the legs during the RPA flights, and using each length scale from 800 m to 6400 m for the sonic anemometers.

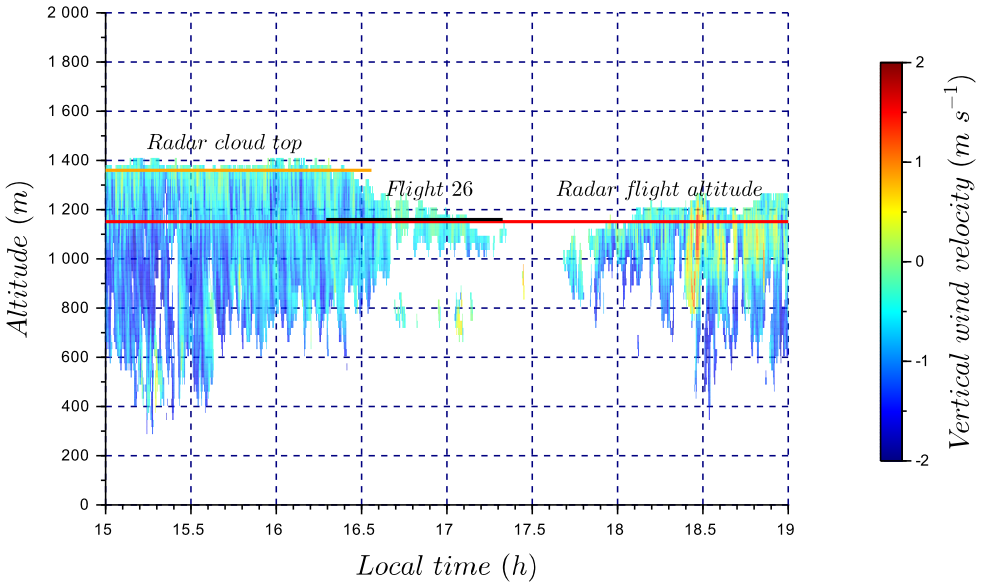


**Figure 11.** Time series of vertical wind velocity for a stratocumulus deck with light precipitation (Flight 26). The color bar represents the cloud radar vertical wind velocity. Flight 26 sampling time is identified by the black segment. The red horizontal line corresponds to radar data at the altitude of the RPA (1160 m.asl), and the orange line corresponds to radar data at cloud top (1360 m.asl). Cloud radar vertical wind velocity at 1160 m.asl and 1360 m.asl are used in Fig.12 to compare with RPA measurements.

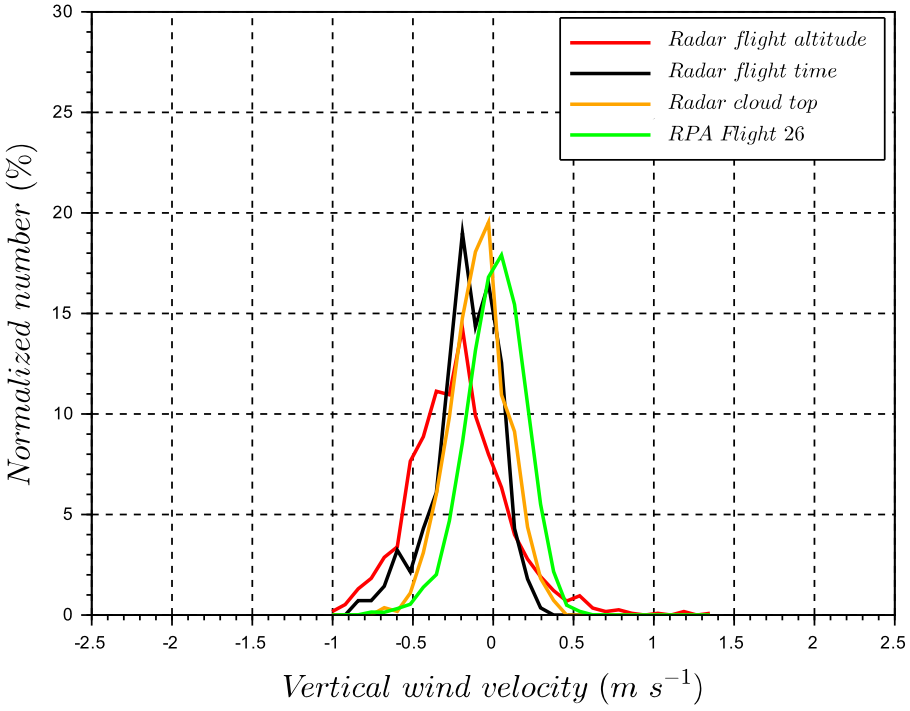


**Figure 12.** A comparison of vertical wind velocity distributions in a lightly precipitating stratocumulus deck between RPA (1160 m.asl) and cloud radar at RPA altitude (1160 m.asl) for 4 h and flight time periods, and cloud radar at cloud top (1360 m.asl).

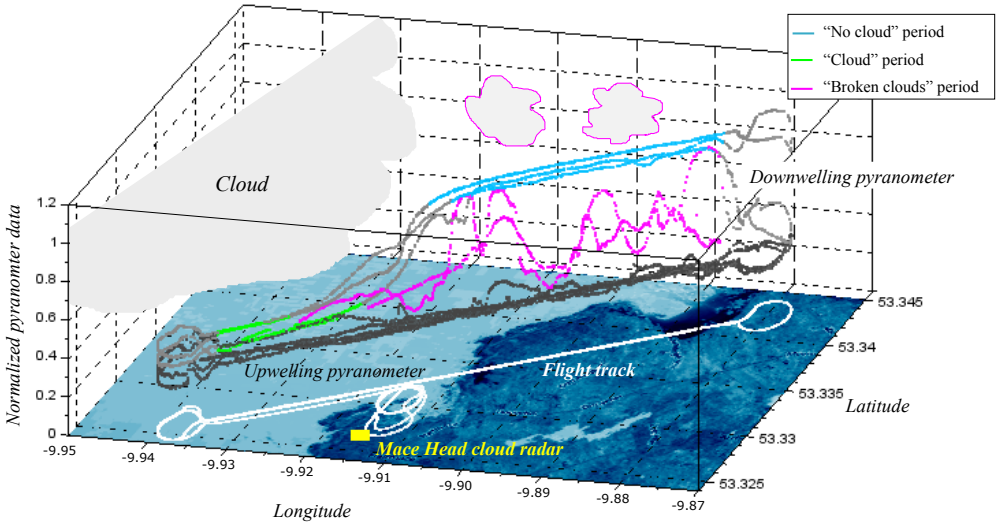


**Figure 13.** Coastal map and flight tracks for the case study of a convective cloud with changing meteorology (Flight 38). Downwelling and upwelling pyranometers data are color-coded based on the three flight periods ("cloud", "no cloud" and "broken clouds"). The developing field of broken clouds (magenta contour clouds) appeared during the last two legs. The cloud radar (yellow square) operated at the Mace Head Research Station.

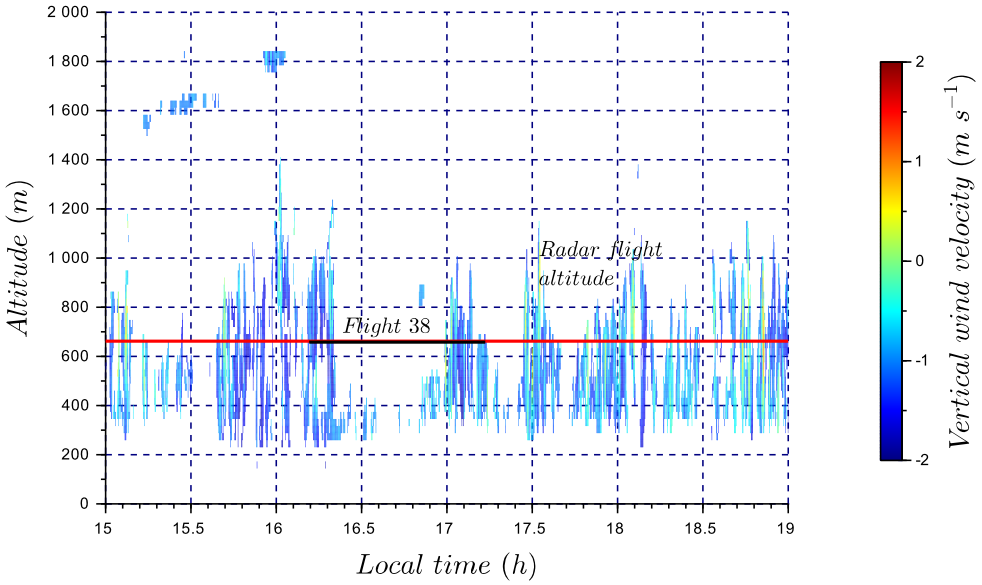


**Figure 14.** Time series of vertical wind velocity associated with Flight 38. The color bar represents the cloud radar vertical wind velocity. Flight 38 sampling time is identified by the black segment. The red horizontal line corresponds to radar data at flight altitude (660 m.asl), used to plot vertical wind velocity distributions in Fig.15.

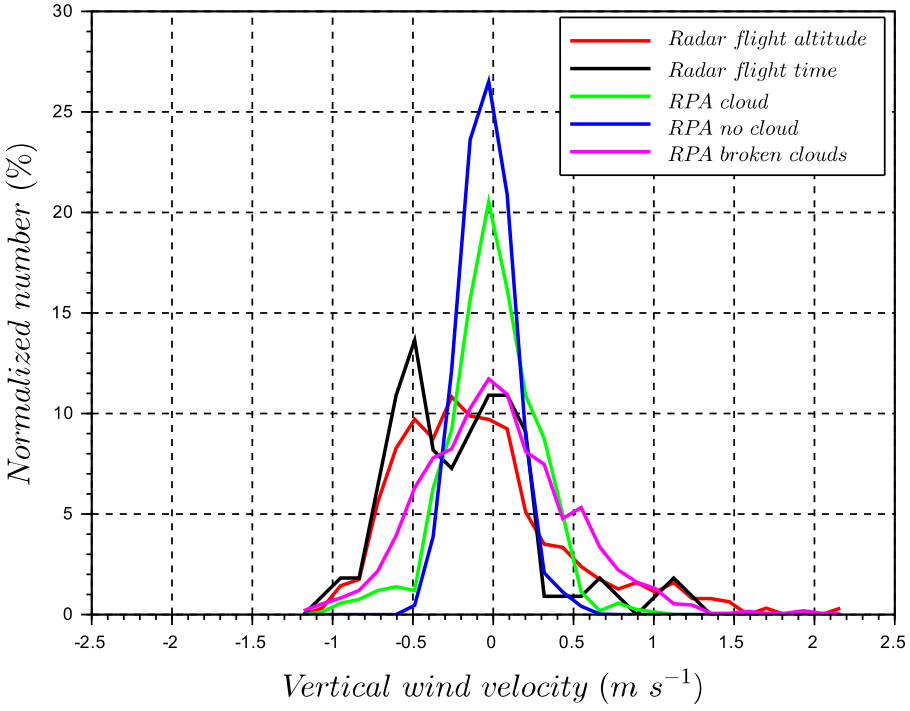


**Figure 15.** Comparison of vertical wind velocity distributions for RPA and cloud radar for Flight 38 at RPA flight altitude from Fig.14. RPA measurements are divided into periods defined in Fig.13 ("cloud", "no cloud" and "broken clouds" periods). The cloud radar detected cloud only for the "broken clouds" period during the RPA flight.

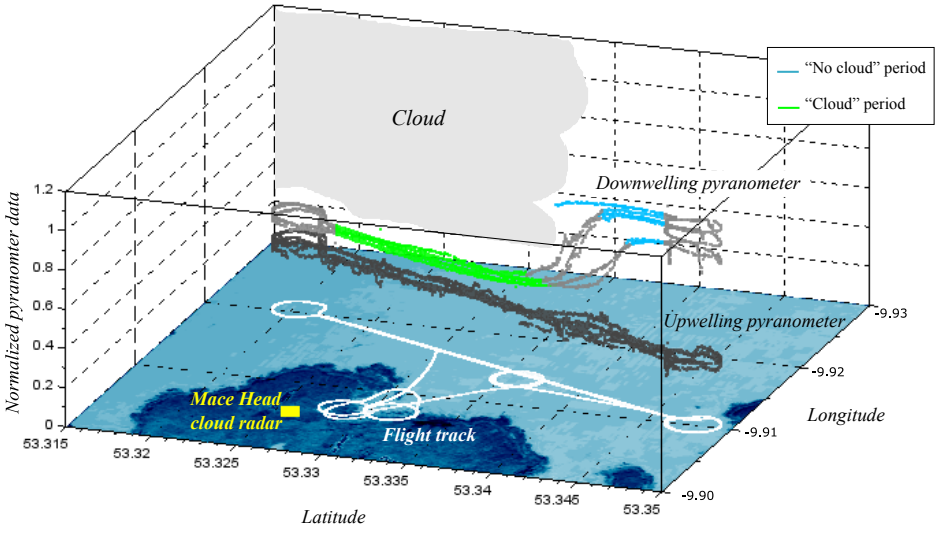


**Figure 16.** Coastal map and flight tracks for the non-convective cloud case study (Flight 30). Downwelling and upwelling pyranometers data are color-coded based on two flight periods, "cloud" and "no cloud" periods. The cloud radar (yellow square) operated at the Mace Head Research Station.

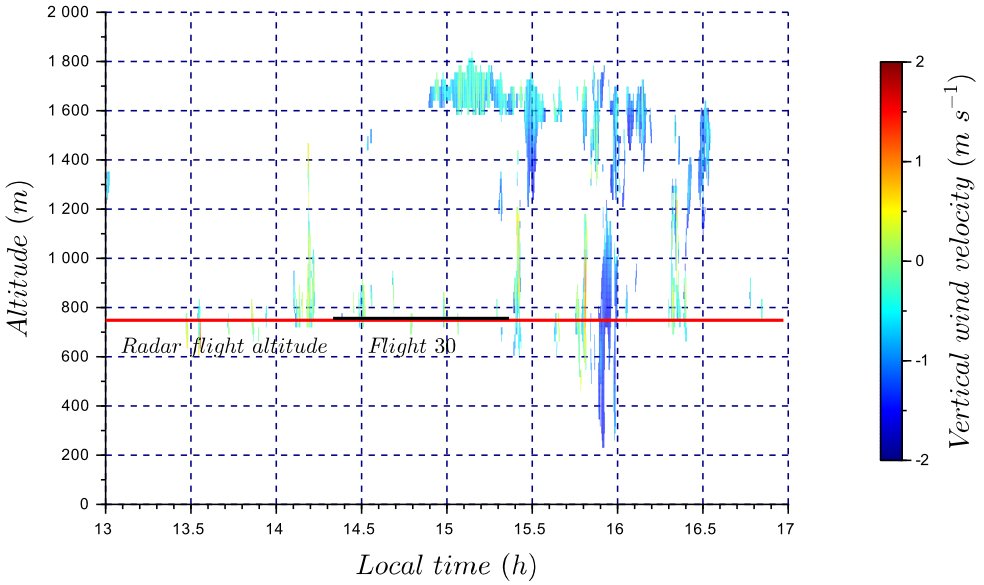


**Figure 17.** Time series of vertical wind velocity associated with Flight 30. The color bar represents the cloud radar vertical wind velocity. Flight 30 sampling time is identified by the black segment. The red horizontal line corresponds to radar data at flight altitude (750 m.asl) used in Fig.18 to plot vertical wind velocity distribution.

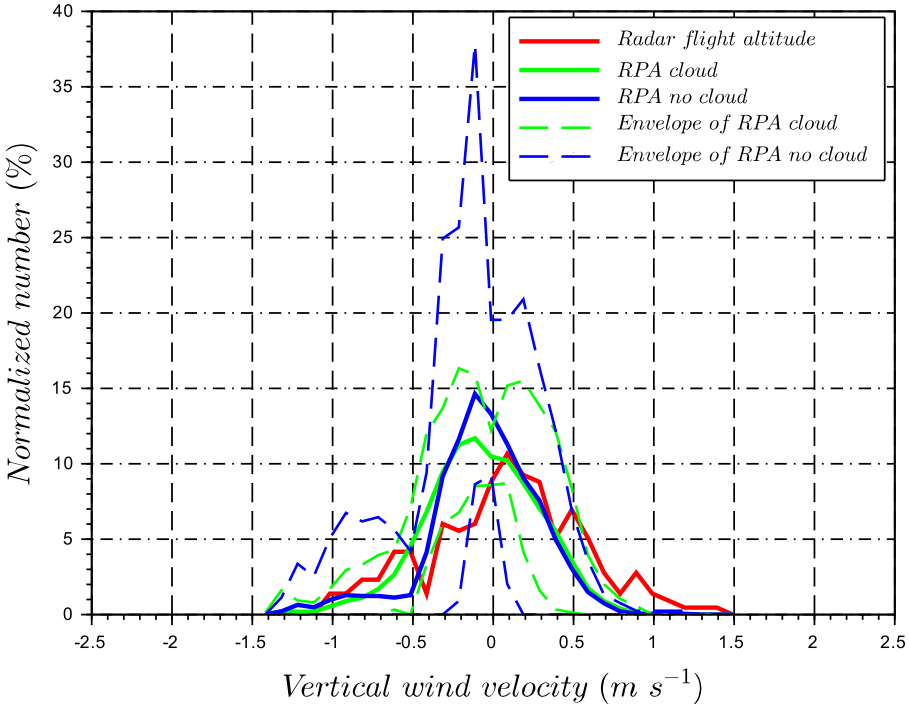


**Figure 18.** Comparison of normalized vertical wind velocity distributions for RPA during Flight 30 and cloud radar at RPA flight altitude (750 m.asl; Fig.17). RPA measurements are divided into "cloud", and "no cloud" periods. The envelope of each period is plotted based on the minimum and maximum number per bin vertical velocity distributions on a leg-by-leg basis.